PCCP

PERSPECTIVE

Cite this: *Phys. Chem. Chem. Phys.*, 2014, **16**, 20360

Electrocatalysis of formic acid on palladium and platinum surfaces: from fundamental mechanisms to fuel cell applications

Kun Jiang,†[a] Han-Xuan Zhang,†[a] Shouzhong Zou*[b] and Wen-Bin Cai*[a]

Received 17th July 2014,
Accepted 13th August 2014

DOI: 10.1039/c4cp03151b

www.rsc.org/pccp

Formic acid as a natural biomass and a CO_2 reduction product has attracted considerable interest in renewable energy exploitation, serving as both a promising candidate for chemical hydrogen storage material and a direct fuel for low temperature liquid fed fuel cells. In addition to its chemical dehydrogenation, formic acid oxidation (FAO) is a model reaction in the study of electrocatalysis of C1 molecules and the anode reaction in direct formic acid fuel cells (DFAFCs). Thanks to a deeper mechanistic understanding of FAO on Pt and Pd surfaces brought about by recent advances in the fundamental investigations, the "synthesis-by-design" concept has become a mainstream idea to attain high-performance Pt- and Pd-based nanocatalysts. As a result, a large number of efficient nanocatalysts have been obtained through different synthesis strategies by tailoring geometric and electronic structures of the two primary catalytic metals. In this paper, we provide a brief overview of recent progress in the mechanistic studies of FAO, the synthesis of novel Pd- and Pt-based nanocatalysts as well as their practical applications in DFAFCs with a focus on discussing studies significantly contributing to these areas in the past five years.

1. Introduction

Electro-oxidation of formic acid (FA) on Pt and Pd electrodes has attracted much attention since the 1960s,[1–3] mainly due to its importance in the understanding of the oxidation of methanol and formaldehyde, as well as the development of direct formic acid fuel cells (DFAFCs).[4,5] DFAFCs possess the advantages of high power density, fast oxidation kinetics, high theoretical cell potential and mild fuel crossover.[6–9] Nevertheless, large-scale commercialization of DFAFCs is hindered by challenging issues such as the low catalytic activity on Pt at low potentials, long-term instability (or deactivation) of Pd and Pt catalysts, degradation of carbon supports and the Nafion membrane, and water–CO_2 management in the fuel cell stacks. Great efforts are being contributed to address these problems through various approaches, such as developing new designs of DFAFCs and screening high efficiency anode catalysts.

Several review articles on FA electrooxidation have appeared in the last few years. In these papers,[6–9] the focus is mainly on the applications of different anode catalysts and the corresponding fuel cell performances. Recently, with the aid of *in situ* techniques, especially attenuated total reflection surface-enhanced infrared absorption spectroscopy (ATR-SEIRAS), and density functional theory calculations, new insights into the FA electrooxidation have been obtained. Meanwhile, highly efficient novel Pt- and Pd-based nanocatalysts have been synthesized. In this review, by discussing selected publications appeared in the past five years and our recent efforts in electrochemical spectroscopic studies and nanocatalyst synthesis, we intend to present an overview of how the achievements in the fundamental studies aid the design of practical nanocatalysts and how the "synthesis-by-design" concept is realized. New developments in DFAFC stack design are also summarized from a holistic point of view.

2. The fundamental aspects

The simple dual pathways are widely recognized for the net decomposition of FA, namely, dehydrogenation (direct pathway), and dehydration (indirect pathway) as shown in the following equations:[1]

Direct pathway:

$$\mathrm{HCOOH} \rightarrow \text{active intermediate} \rightarrow \mathrm{CO_2} + 2\mathrm{H^+} + 2\mathrm{e^-} \quad \text{(electrooxidation)} \quad (1)$$

$$\rightarrow \mathrm{CO_2} + \mathrm{H_2}\ \text{(self-dehydrogenation)} \quad (2)$$

[a] *Shanghai Key Laboratory for Molecular Catalysis and Innovative Materials, Department of Chemistry, Fudan University, Shanghai 200433, China. E-mail: wbcai@fudan.edu.cn; Fax: +86-21-65641740; Tel: +86-21-55664050*

[b] *Department of Chemistry and Biochemistry, Miami University, Oxford, OH 45056, USA. E-mail: zous@miamioh.edu*

† These authors contributed equally to this work.

Indirect pathway:

$$HCOOH \rightarrow CO_{ad} + H_2O \quad (3)$$

The former pathway may yield CO_2 from an active intermediate adsorbed on a metal catalyst surface at the open circuit potential (OCP) through simple decomposition of FA[10] or through electrooxidation at higher potentials. On the other hand, the latter pathway leads to CO species strongly adsorbed on the electrode surface, especially on Pt, and severely blocks the active sites for the dehydrogenation pathway at low potentials.

In the past decade, fundamental studies of formic acid oxidation (FAO) on Pt and Pd mainly focused on three aspects: (i) clarifying the chemical nature of the active intermediate in the direct pathway, (ii) diminishing CO adsorption on Pt electrodes and (iii) understanding whether and how CO_{ad} form on Pd catalysts. These fundamental investigations yield new insights into the FAO process on Pt and Pd catalysts which form the basis of design rules for tailor-made high efficiency catalysts. In the following we summarize these new findings and discuss the unresolved issues in understanding the FAO mechanism.

2.1 Reactive intermediate of FAO (controversy over formate)

With regard to the reactive intermediate of FA oxidation on Pt electrodes, it has been long assumed that a carboxylic acid species adsorbed *via* the carbon atom (–COOH)[11,12] is the rate-determining intermediate for the direct pathway until Osawa's group first successfully detected the adsorbed formate (HCOO) by ATR-SEIRAS[13] on a chemically deposited Pt film electrode. Recently, formate was also clearly identified on Pd electrodes by the same group using the same technique at sufficiently high potentials.[14]

Although the detection of formate may largely exclude other carboxylic species as the reactive intermediate, the role of formate in the direct pathway remains controversial. Osawa's group initially proposed that this species is involved in the rate determining step based on detailed *in situ* electrochemical ATR-SEIRAS investigations, which means the oxidation of FA to CO_2 *via* adsorbed formate on Pt electrodes.[15–17] They suggested that the oxidation current of FA through the direct pathway may be described by the following equation:

$$i \propto -\frac{d\theta_{formate}}{dt} = k\theta_{formate}(1 - \theta_{CO} - 2\theta_{formate}) \quad (4)$$

where i is the current, k is the rate constant, and $\theta_{formate}$ and θ_{CO} are coverages of formate and CO (including CO_L and CO_B), respectively. This equation implies that formate adsorbs on the Pt surface in the bridge-bonded way and its oxidation relies on the presence of adjacent vacant sites for C–H bond scissoring.

More recently, Cuesta *et al.*[18,19] claimed that the adsorbed formate is the key intermediate in both the dehydrogenation and dehydration pathways and bimolecular decomposition of adjacent adsorbed formate with a subsequent electron transfer contributes to the oxidation current in the dehydrogenation pathway on Pt and Au, suggesting that no free metal site is necessary for formate oxidation. In addition to spectral evidence, Grozovski *et al.*[20] demonstrated that the current for FA oxidation is directly proportional to the formate coverage on Pt single crystal electrodes by comparing the charge for adsorbed formate and the recorded oxidation current.

The assignment of formate as a reactive intermediate was disputed by Chen *et al.*[21–25] who studied FAO on Pt electrodes using the same technique but coupled with a thin-layer electrochemical flow cell. The flow cell configuration facilitates the quantitative analysis of the IR signal of adsorbates in the electrocatalytic reactions under well-defined mass-transport conditions. Based on their results, Chen *et al.* argued that formate is a spectator rather than a reactive intermediate and proposed a so-called "three pathway" mechanism for FA oxidation. By using simultaneous ATR-SEIRAS and cyclic voltammetry, Okamoto *et al.* further excluded the possibility of bridge-bonded formate ($HCOO_B$) as the reactive intermediate by carefully analyzing the effect of the scan rate on potential dependent formate band intensity and oxidation current.[26] This argument was to some extent supported by the DFT calculations of Neurock *et al.*[27] who suggest that the adsorbed formate is relatively stable while an experimentally undetectable *COOH intermediate is the active intermediate.

On the other hand, Wang *et al.*[28] reported DFT calculations of FA oxidation on the Pt(111)/H_2O interface with a continuum solvation model and showed that formate is neither a reactive intermediate nor a spectator for FA oxidation, but a template that promotes the adsorption of FA in a CH-down configuration, which is a reactive precursor leading to CO_2. Gao *et al.* suggested a dual-path mechanism involving a formate pathway *via* the $HCOO_B$* intermediate and a direct pathway from HCOOH* *via* a highly transient COO* intermediate by first principle simulations.[29,30] In a newly modified mechanism proposed by Osawa's group, formate ions rather than formic acid molecules are oxidized *via* a weakly adsorbed formate precursor,[31–33] and both the adsorbed OH species and $HCOO_B$ can suppress $HCOO^-$ oxidation by blocking active surface sites. Most recently, Chen's group proposed that the oxidative adsorption of formic acid is the rate-determining step and that the reactive intermediate in the direct pathway is ascribed to the corresponding unspecified X^- species, based on a potential oscillation modeling on the Pt electrode.[34] Summarized in Fig. 1 are typical mechanisms proposed.

The mechanism of formic acid oxidation is far from settled, in particular, the chemical nature of the reactive intermediate. The assumption that adsorbed –COOH is the reactive intermediate lacks spectral evidence.[12,27] While a weakly-adsorbed HCOOH precursor can explain a kinetic isotope effect for HCOOH and DCOOH oxidation to CO_2,[21] a weakly adsorbed $HCOO^-$ precursor can explain a pH dependence of oxidation current.[31] However, the former is difficult to explain the pH dependence because the concentration of formic acid decreases with an increase in the solution pH. *Vice versa*, the latter is hard to explain the kinetic isotope effect given that the rate-determining step is the adsorption of $HCOO^-$.

A recent trend in discussing the mechanism of formic acid electro-oxidation involves dual species collaboration. For example,

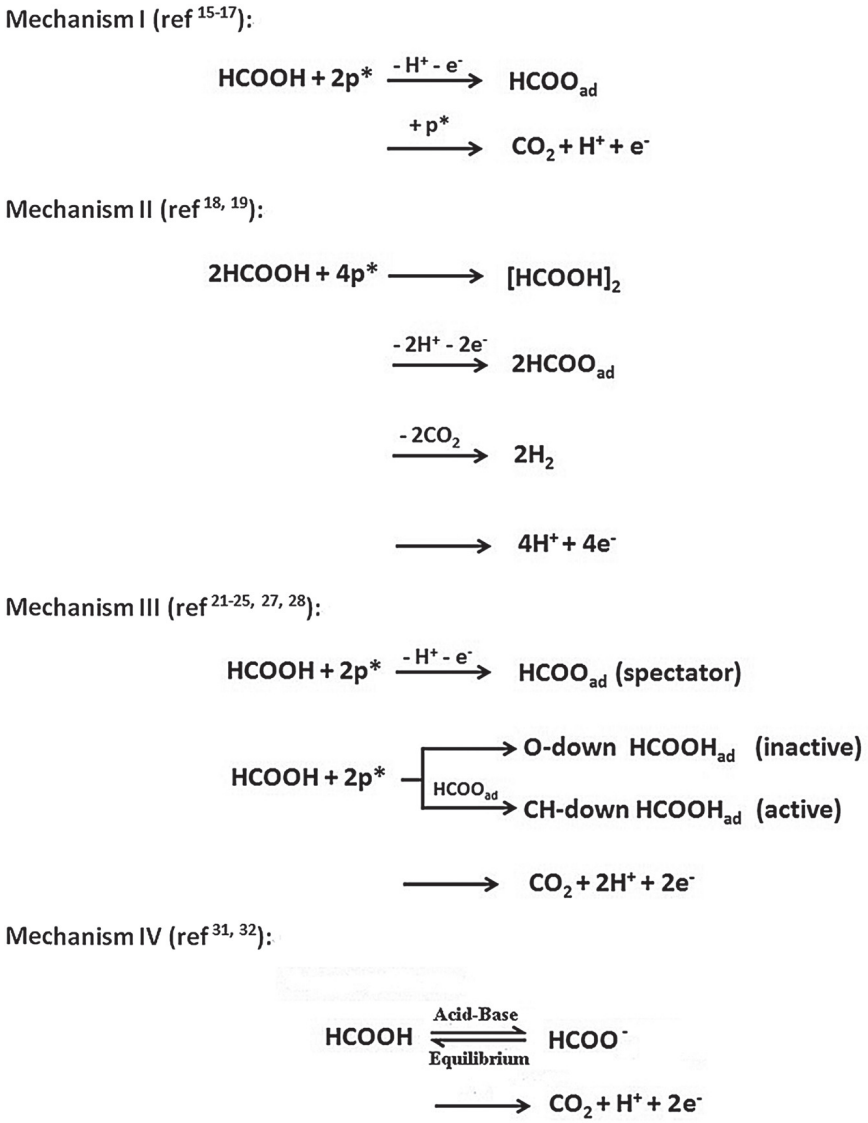

Fig. 1 Proposed dehydrogenation pathways of FA oxidation in the literature. p* refers to the empty metal surface sites required for the reaction.

Herrero *et al.*[35,36] explained the pH and anion (sulfate, perchlorate or acetate) effects on FAO at the Pt(111) electrode by combining the formate template model[28] and mechanism IV. Brimaud *et al.*[37] investigated in detail the influence of electrolyte pH, electrode surface structure, and anion adsorption on FA oxidation on Au and Pt electrodes. Distinct differences in the reaction behavior on Pt and Au were observed, as well as in the structural sensitivity and anion effects. They suggested that a dimer-like species probably comprising HCOOH (or $HCOO_{ad}$) and $HCOO^-$ is the reactive intermediate in the dehydrogenation pathway, rather than a single species such as COOH, $HCOO_B$ or $HCOO^-$. The collaborative effect of HCOOH and weakly adsorbed $HCOO^-$ seems extendable to explain self-dehydrogenation of formic acid on carbon supported Pd and B-doped Pd catalysts in a formic acid–formate solution.[38]

2.2 Poisoning intermediate CO

CO formation on three-contiguous Pt sites. Through IR spectroscopic investigations of FA oxidation on Pt electrodes,[39,40] adsorbed CO (CO_{ad}) is identified as the major poisoning species formed through the dehydration pathway. Such CO_{ad} can be removed only at high applied potentials, leading to a significantly suppressed dehydrogenation pathway and low catalytic activity at lower potentials. Because the dehydrogenation pathway is highly desired for the best utilization of the chemical energy stored in FA, many efforts have been made to promote this pathway.

On Pt electrodes, it is widely accepted that the ''ensemble effect'' or ''third-body effect'' plays an important role in improving the FA oxidation performance, which has been extensively reviewed by Markovic and Ross.[41] The concept of the ''ensemble effect'' was initially borrowed from the hydrocarbon catalysis on Bi modified Pt surfaces,[42] referred to the effect that a reaction requiring a large ensemble of surface active sites can be suppressed by diluting the active sites with a second inert metal, the so-called ''third-body''. Thus, in the case of FA dehydration on Pt electrodes, the determination of the smallest number of surface

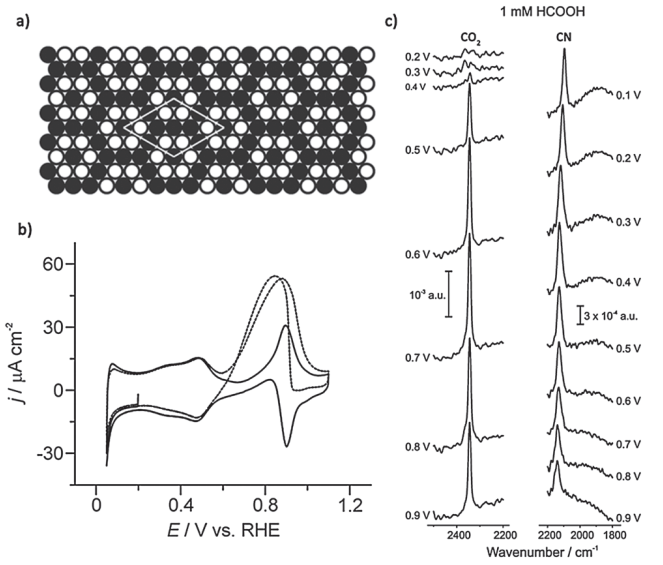

Fig. 2 (a) The ball model of the cyanide-modified Pt(111) electrode (black balls correspond to Pt atoms, and white balls correspond to linearly chemisorbed –CN groups). (b) Cyclic voltammograms of a cyanide-modified Pt(111) electrode in 0.1 M $HClO_4$ + 1 mM HCOOH (solid line) and 0.1 M $HClO_4$ + 0.2 M HCOOH (dashed line) and (c) the corresponding FTIR spectra at increasing potentials obtained in the first solution (reprinted with permission from ref. 43. Copyright 2009, American Chemical Society).

"ensemble" Pt atoms and their geometric arrangement required for this reaction may help to channel the FA oxidation route to the direct pathway by fabricating a surface unfavorable for CO_{ad} formation. Combining cyclic voltammetry (CV), FT-IR spectroscopy and differential electrochemical mass spectrometry, Cuesta *et al.*[43] reported that CO_{ad} is almost inhibited on a cyanide-modified Pt(111) during FA oxidation and the corresponding electro-oxidation reaction proceeds exclusively through the dehydrogenation pathway (shown in Fig. 2). Because cyanide adsorption on Pt(111) forms a hexagonally packed structure which contains six –CN groups adsorbed atop of six Pt atoms surrounding a free Pt atom, their results suggest that CO_{ad} formation due to the dehydration pathway would require the presence of at least three contiguous Pt atoms. This conclusion also coincides with the DFT calculations by Neurock *et al.*,[27] which suggest that the direct pathway appears to occur over just one or two Pt atoms while the indirect path requires a significantly greater ensemble size and defect sites. The enhanced FA oxidation catalytic activity and suppressed CO_{ad} coverage were also confirmed on the Sb[44,45] or Bi[46] modified Pt single crystal electrodes, respectively.

Interestingly, this ensemble effect has been recently challenged by Grozovski *et al.*[47] with electrochemical studies on a series of Pt single crystal electrodes. They suggested that no CO_{ad} would form on a perfect Pt(111) electrode and the observed CO_{ad} comes from the defect sites. When the Pt(111) surface is modified with cyanide, the defects are blocked and consequently, no poison is detected.

Recently, we applied high sensitivity *in situ* EC-SEIRAS together with a DFT calculation to investigate the mechanism of FA electro-oxidation on a Sb-modified Pt polycrystalline electrode[48] and provide some new insights into the role of adatoms on Pt surfaces. Our results show that the FA oxidation current is not correlated with the formate coverage, and the Sb-modification decreases the CO coverage significantly. On the basis of the periodic DFT calculations, the catalytic role of Sb adatoms can be rationalized as a promoter for the adsorption of the CH-down configuration but an inhibitor for the adsorption of the O-down configuration of formic acid, facilitating the complete oxidation of FA to CO_2 (Fig. 3). In addition, Sb modification lowers the CO adsorption energy, and helps to mitigate the CO poisoning effect on Pt. The decreased CO_{ad} coverage during FA oxidation was also demonstrated on Au cluster-modified Pt monolayers on a nanoporous-gold electrode by ATR-SEIRAS measurements.[49]

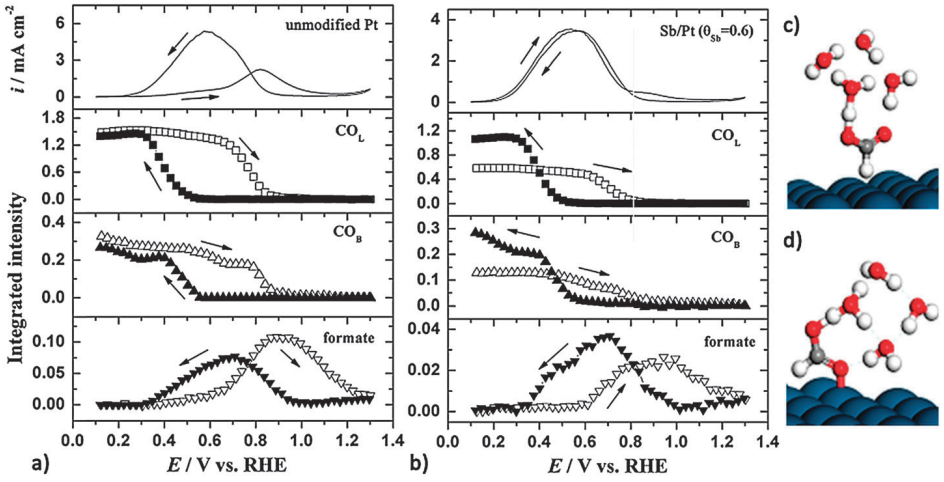

Fig. 3 Cyclic voltammograms of unmodified Pt (a) and Sb-modified Pt (b) electrodes in 0.5 M H_2SO_4 + 0.1 M HCOOH solution recorded at 10 mV s^{-1} and the integrated intensities of CO_L, CO_B, and formate selected from the corresponding time-resolved SEIRAS spectra recorded simultaneously with the CVs. The CH-down (c) and O-down (d) configurations of HCOOH adsorption on Pt(111) (reprinted with permission from ref. 48. Copyright 2010, American Chemical Society).

CO formation from CO_2 reduction on Pd surfaces (deactivation of Pd surfaces). It has been widely recognized that the dehydration pathway of FA oxidation is not much favored on the Pd-based electrode surfaces and the absence of CO poisoning leads to a much higher initial catalytic activity on Pd at lower potentials as compared to that on Pt surfaces.[3] Recently, a DFT calculation also confirmed CO_2 as the dominant product for FA decomposition on Pd(111) surfaces.[50] In 2004, Masel's group[51] first explored the use of Pd black as an alternative anode catalyst for DFAFCs and demonstrated significant performance enhancements. Further investigations reveal that the deactivation during FA oxidation is a severe obstacle of Pd catalysts for their practical applications.[6,7] Hence much efforts have been paid to disclose the nature of the deactivation process.

Diverse proposals have been put forward to explain the deactivation during (electro)chemical dehydrogenation of FA on Pd surfaces such as the aggregation of Pd nanoparticles[52] and surface blocking by the CO_2 bubbles.[53] Other than these physical inhibitions, another important suggestion points to the accumulation of inactive (poisoning or spectator) intermediates on surfaces. In 1988, Solis *et al.*[54] studied FAO on Pd electrodes with on-line mass spectroscopy and suggested the presence of strongly adsorbed residues at a small coverage. By using electrochemical impedance spectroscopy (EIS), Uhm *et al.*[55] and Jung *et al.*[52] further confirmed the presence of the strongly adsorbed residue. Recently, anodic stripping measurements[52,56,57] on carbon supported Pd nanoparticles that were pre-polarized in a concentrated FA solution for hours and then transferred to a $HClO_4$ solution revealed the presence of so-called "CO_{ad}-like residues" on Pd surfaces. It was also reported that the existence of Pd–O(H) species[58] or the application of a positive potential treatment[52,59,60] to the Pd electrode may facilitate the removal of such "CO-like" species and hence recover the performance of a DFAFC.

In contrast, CO_{ad} was not detected on ultrathin Pd overlayer(s) on Pt[61] or Au[62] electrodes in the electrooxidation of FA at varying potentials with external IRAS and ATR-SEIRAS, respectively. Neither was it identified on Pd(111) in a highly concentrated FA solution.[63] In a recent ATR-SEIRAS study,[14] by using a chemically deposited Pd film on the Si prism as the working electrode in a 25 mM FA solution, Miyake *et al.* detected very weak CO_{ad} peaks around 1730 cm^{-1} at relatively low oxidation potentials while even weaker peaks around 1830 cm^{-1} appeared as the potential was scanned to higher values. However, such an assignment may be compromised due to the possible overlapping of the $\nu_{C=O}$ vibration band (at *ca.* 1720 cm^{-1}) of interfacial FA.[62] Moreover, the chemically deposited Pd electrode was easily broken and peeled off from the Si prism with increasing hydrogen absorption, limiting its working electrode potential to be positive of 0.2 V (RHE).

Recently, we applied *in situ* ATR-SEIRAS combined with thin layer flow cell configurations to study the decomposition of HCOOH on Pd surfaces over a potential range of practical relevance to the hydrogen production (*i.e.*, at open circuit potential) and fuel cell anode operation.[64] For the first time solid spectral evidence of CO_{ad} formation with the clear vibrational bands located at *ca.* 1850 cm^{-1} was obtained. These CO species can be ascribed to the triple-bonded CO on Pd surfaces with a relatively low coverage (increased with increasing time and decreasing potential). A careful investigation of the effects of mass transport, concentration of FA and supporting electrolyte, electrode potential, and the control measurement on CO_2 reduction enables us to find that the CO_{ad} coverage depends on the surface CO_2 concentration and the electrode potential, and propose that the CO_{ad} may primarily originate from the reduction of the dehydrogenation product CO_2 as illustrated in Fig. 4. This conclusion is further supported by a recent electrochemical study on Au@Pd electrodes[65] with different Pd overlayer thicknesses, which shows that the increasing FA oxidation rate accelerates CO_{ad} poisoning due to CO_2 reduction.

We further extended the ATR-IR spectroscopic technique to study the surface poisoning species on the state-of-the-art commercial Pd black catalyst in FA solutions with much higher concentrations (~5 M) under different potential settings mimicking to some extent the practical DFAFC operation conditions.[66] CO_{ad} was also clearly confirmed as a surface poisoning species with its vibrational frequencies located over ~1848 to 2050 cm^{-1}, suggesting a much higher CO coverage in the concentrated FA solution. This finding is in good agreement with the previous electrochemical measurements[52,67] and demonstrates the capability of the ATR-SEIRAS technique to study practical catalysts. These results provide a molecular level insight into the deactivation of the Pd electrodes during FA

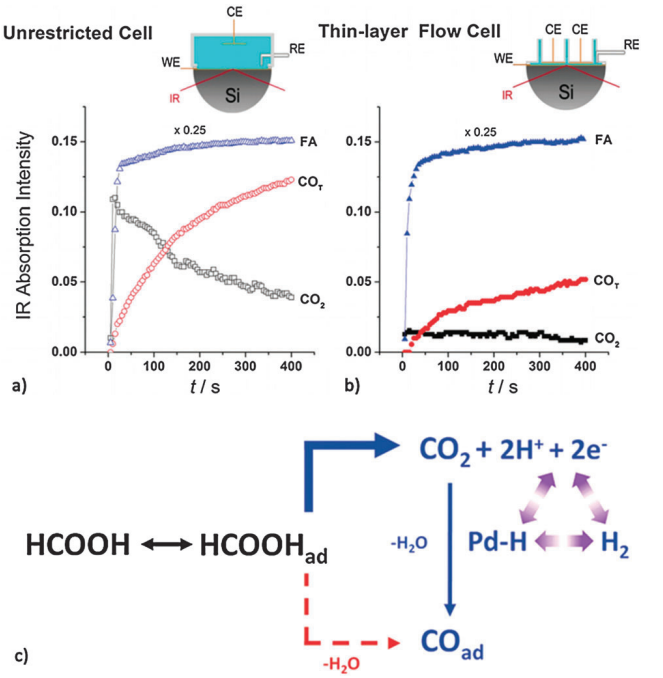

Fig. 4 Evolution of the IR peak intensities related to the near-surface CO_2 product and interfacial FA molecules in the solution phase as well as the adsorbed CO_T species on Pd surfaces recorded at the OCP in 0.1 M $HClO_4$ + 0.5 M FA collected in a regular unrestricted ATR cell (a) and a thin layer flow cell (b). (c) Reaction scheme from HCOOH to CO_{ad} on a Pd surface including the reduction of the dehydrogenation product CO_2 (reprinted with permission from ref. 64. Copyright 2011, American Chemical Society).

oxidation and highlight the critical importance of anti-CO poisoning and CO_2 management when Pd-based catalysts are designed and used for practical applications.

3. Catalysts for electrooxidation of formic acid

Parallel to the mechanism study of the FA electrooxidation on Pt- and Pd-based surfaces, many novel nanocatalysts with higher catalytic activity, durability and lower cost have also emerged. Attempts have been made to tailor the electronic properties and construct the optimal catalytic structure using the ''synthesis-by-design'' concept.

3.1 The main principles of ''synthesis-by-design''

''Third-body'' effect. As mentioned above, the most effective way to channel the FAO pathway on Pt electrodes to the dehydrogenation path is to form a surface unfavorable to CO_{ad} formation through the ''third-body'' effect by modifying the Pt surface with a second metal. In the catalyst design, the ''third-body'' ad-atoms such as Sb, Pb and Bi formed by irreversible adsorption or underpotential deposition (UPD) are effective for creating discontinuing Pt sites and thus hinder the CO formation (*i.e.*, the indirect pathway).[7,68–72] Successes have also been achieved by alloying Pt with other metals, such as Au,[73–76] Ag,[77] Fe[78,79] and Cu.[80] In 1980s, Watanabe *et al.*[69] reported that FA oxidation was enhanced by three orders of magnitude on Pt electrodes by ad-atoms of the Vth group metals. However, an agreement on the optimal coverage of the ad-atoms on Pt electrodes has not been reached, probably due to different surface Pt sites, ad-atoms and modification methods applied in the previous reports. By introducing these concepts to the fabrication of nanomaterials, high efficiency Pt-based nanocatalysts can be obtained as summarized in Section 3.3.

Electronic effect. When pure Pt or Pd is alloyed or modified with a second metal, the change in the surface atomic environment is inevitably accompanied by the change in their valence electronic structure. A particularly useful model to illustrate such a variation in the electronic structure of transition metal surfaces is the so-called d-band theory, which is widely used in heterogeneous catalysis (including electrocatalysis).[81] As extensively reviewed by Demirci,[82] Nørskov and co-workers[83–85] pioneered in using the d-band center (ε_d) shift as the simplest descriptor to indicate the variation of electronic structure and binding energies of surface poisoning and reactive intermediates on catalyst surfaces, and explain the corresponding changes in the catalytic reactivity.

Briefly, the position of ε_d is controlled by the shape of the d-band and the number of filled electrons. ε_d is affected by the inter-atomic distance of the metals.[83,86] When Pt or Pd is modified with a second metal with a larger lattice constant, the parent metal is under tensile strain and its d-orbital overlap decreases, which results in a narrower d-band and an up-shifted ε_d, as shown in Fig. 5a (left). Conversely, if the second metal has a smaller lattice constant than Pt or Pd, the overlap of the d-orbital of Pt or Pd increases. As a result, the d-band becomes broader and the d-band center decreases (Fig. 5a, right). These effects are termed the strain effect. By tuning the d-band center of the pseudomorphic Pd monolayer on various single crystal electrodes with different lattice constants, Kibler *et al.*[87] experimentally testified the correlation between the d-band center position and the catalytic activity towards FA electrooxidation. They disclosed a nearly linear relationship between the binding energy (*i.e.* the oxidation peak potential) of adsorbed hydrogen and the calculated shift of the d-band center of the Pd overlayer on different single crystal electrodes as shown in Fig. 6a and b. The best FAO catalytic performance was obtained on the $Pd_{ML}/Pt(111)$ and $Pd_{ML}/PtRu(111)$ electrodes (Fig. 6c). Such an improvement in the catalytic ability may be attributed to the facilitation of an intermediate adsorption/desorption balance during FA oxidation with a suitable down-shift of the Pd d-band center and corresponding binding energy of the intermediate. This work provides an interesting way of screening metals alloyed with Pd or Pt for FA oxidation, and opens an avenue for the design of novel high efficiency nanocatalysts.

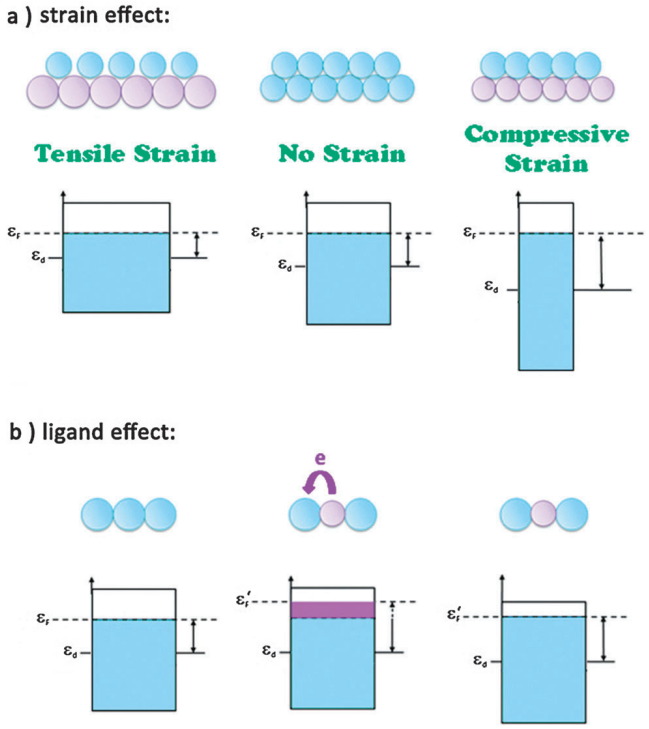

Fig. 5 Schematic description of the strain effect (a) and the ligand effect (b) in bimetallic catalysts when an adlayer or an alloyed structure is formed.

The subtle down-shift of the d-band center can also be caused by the ligand effect (Fig. 5b). According to Nørskov's DFT calculation,[82] the d electrons in less noble metals such as Ni, Co, Fe and Ag tend to transfer to Pt or Pd which consequently down-shifts the d-band of the latter. This finding provides some hints for designing new catalysts. Wakisaka *et al.*[88] demonstrated experimentally that when Pt is alloyed with Co or Ru the electron transfer occurs from the latter to Pt through the so-called ''ligand effect'', resulting in a down-shift of the d-band center of Pt due to the down-shift of the reference level

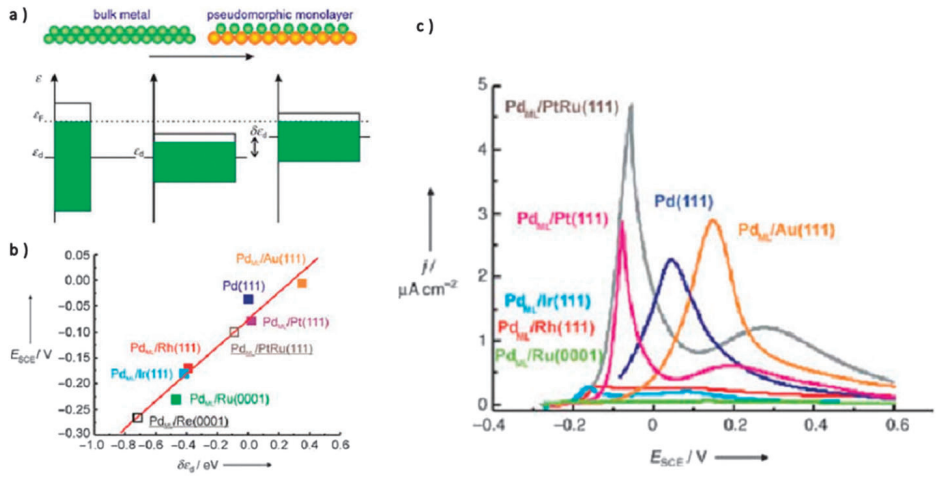

Fig. 6 (a) d-band center shift model of pseudomorphic palladium monolayers (Pd_{ML}); (b) linear relationship between the oxidation potential of adsorbed hydrogen and the calculated d-band center shift of Pd_{ML} on various single crystal electrodes; (c) the corresponding FAO behavior of the pseudomorphic Pd_{ML} electrodes (reprinted with permission from ref. 87. Copyright 2005, Wiley-VCH).

(or the Fermi Level, ε_F, see Fig. 5b) and a corresponding positive shift of Pt $4f_{7/2}$ core level binding energy in the XPS measurements. It should be pointed out that the strain effect and the ligand effect are hard to be separated in practical bimetallic catalysts and the "net" d-band center shift is more important for designing better catalysts.

Facet-dependent catalytic activity. Facet-dependent electrocatalysis is another important issue in catalyst design.[89] In a typical cyclic voltammetric test, the FA oxidation current is greatly inhibited due to the surface blockage by CO during the positive scan on Pt(110) and Pt(100) electrodes, while the Pt(111) is not much affected. After CO is oxidized at the high potentials, the Pt(100) electrode shows the best catalytic activity toward FAO during the backward scan with the corresponding peak oxidation current 5–6 times larger than that on Pt(111) and Pt(110) electrodes.[41,47,90,91] However, such a facet-dependent catalytic activity of Pt has not been extensively applied to the design of nanocatalysts.

Hoshi *et al.*[92,93] systematically studied the structural effects of FAO on well-defined Pd single crystal electrodes with low and high index planes. On the low-index planes of Pd, the maximum current density of FA oxidation increases in the positive scan as follows: Pd(110) < Pd(111) < Pd(100). For the high index planes, the maximum current density increases in the order of Pd(S)-[n(111) × (111)] < Pd(S)-[n(111) × (100)] < Pd(S)-[n(100) × (110)] < Pd(S)-[n(100) × (111)] and the Pd(511) (=5(100)-(111)) electrode possesses the highest catalytic activity among the high index planes examined. The knowledge learned from these studies on bulk single crystals can be used to design nanoscopic practical Pd catalysts. Different preferred facets may be obtained by controlling the shape of nanocrystals.

3.2 Pd-based catalysts

Pd-based alloy catalysts. Various Pd–M catalysts have been synthesized and they showed attractive performance in the past few years. The second metal M includes but is not limited to Pt, Au, Ag, Cu, Ni, Co, Pb, Sn, Fe and Ir, and normally the electronic effect and strain effect are invoked to account for the activity enhancement.[94–109]

Liu *et al.*[99] reported the promotion effect of Au in the PdAu/C for FA oxidation and the highest activity was obtained when the ratio of Pd : Au is 3 : 1. Similarly, the PdAu/C alloy nanocatalyst[104] synthesized *via* a simple co-deposition strategy exhibit higher Pd-specific activities towards FA oxidation compared with the non-alloy counterparts or unmodified Pd/C catalysts. Pd–Au/C catalysts with different alloying degrees were also tested,[110] in which a higher electrocatalytic activity and stability was in accordance with a high alloying degree as expected. For a practical DFAFC, Larsen *et al.*[94] found that alloying foreign metals such as Au to Pd/C anode catalysts enhanced its performance. Favorable effects have been also detected by alloying Co,[95,96] Sn[97,98] or Ni[108,109] with Pd to form nanocatalysts.

Inspired by the "third-body" effect and the d-band center theory, we synthesized and screened a series of carbon supported Pd_xPt_{1-x} nanocatalysts in order to pinpoint the optimal composition for the electrocatalytic oxidation of FA.[101] As shown in Fig. 7, $Pd_{0.9}Pt_{0.1}$/C has the highest peak current among all of the tested samples, which can be attributed to the effective alleviation of CO formation at separated Pt sites, and the appropriately lowered d-band center of Pd sites for optimal reactant and intermediate adsorption. Similar results were also obtained on a series of Pd–Pt nanocatalysts with a Pt content less than 10%, including the Au@Pd–Pt nanocubes,[103] Pd–Pt alloy nanocubes,[100] tetrahexahedral Pd–Pt alloy catalysts[106] and Pt decorated Pd/C nanoparticles.[105] Along this line, ternary nanoalloys of Pd–Pt–M with a low Pt content, *i.e.*, Pd–Pt–Au/C[111] and Pd–Pt–Cu/C[112] exhibited more flexibility than binary nanoalloys in tuning the electronic properties of catalytic surfaces, and thus provided a more balanced improvement on both the activity and durability.

In addition to the metallic alloying components, non-metals such as P and B can also be applied as the additives to Pd

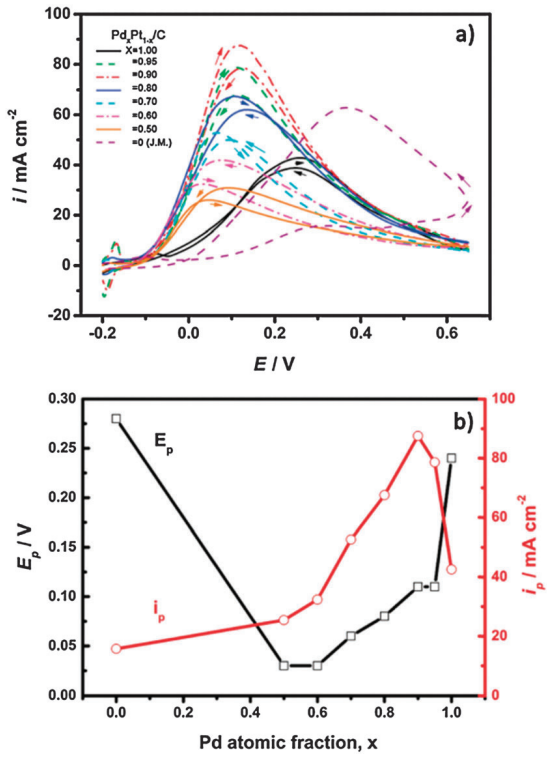

Fig. 7 (a) Cyclic voltammograms recorded at 50 mV s^{-1} for Pd_xPt_{1-x}/C-coated GC electrodes in 0.5 M H_2SO_4 solution containing 0.5 M FA; (b) variation of E_p and i_p with Pd molar fraction x (reprinted with permission from ref. 101. Copyright 2010, American Chemical Society).

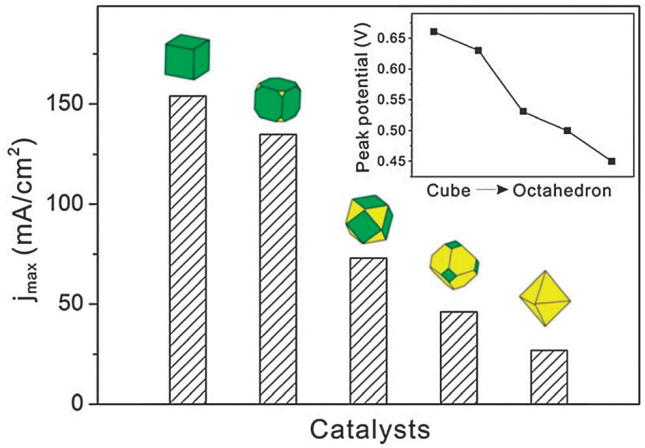

Fig. 8 Maximum current densities of HCOOH oxidation on Pd polyhedra enclosed by {111} and {100} facets in different proportions (reproduced from ref. 118 with permission from The Royal Society of Chemistry).

catalysts to increase their catalytic activity. By using either NaH_2PO_2[113] or phosphorus[114] as the reductant as well as a direct P donor, Lu *et al.* successfully prepared Pd–P metal–nonmetal alloy nanocatalysts, which show a much better catalytic performance as compared to the pure Pd. Pd–B/C catalysts (*ca.* 40 wt% Pd with 6 at% B doping) were also synthesized through an aqueous process using dimethylamineborane as the reducing agent[38,115] and showed enhanced activity and poison resistance toward formic acid (self)dehydrogenation.

Modification of Pd surfaces with ad-atoms is an alternative way to achieve high catalytic activity and high resistance to poisoning species.[116,117] Haan *et al.*[117] found that Sb ad-atoms can double the rate of FA oxidation on Pd surfaces. The same group[116] further screened the effects of Sb, Sn, and Pb ad-atoms on Pd black catalysts in the fuel cell operation test, and discovered that all of these ad-atoms strongly promote FA oxidation and reduces the amount of CO. The synergetic and electronic effects were suggested to be responsible for such an enhancement.

Pd nanocrystals. The facet-dependent electrocatalytic activity towards FA oxidation of the Pd nanocrystals has also been explored. Jin *et al.*[118] prepared Pd nano-polyhedrons with different shapes, including truncated cubes, cuboctahedra, truncated octahedra and octahedra, by controlling the growth of cubic seeds. As shown in Fig. 8, FA oxidation over these Pd polyhedra were systematically studied, and a decline in maximum current density and a negative shift of peak potential were observed when the area ratio of 100{100} to {111} facets on the surfaces of a Pd polyhedron decreased. More recently, we presented a simple one-pot synthesis method to selectively synthesize either Pd rhombic dodecahedra or cubic NCs of similar sizes.[119] By applying a mild CO-replacement cleaning process to remove the surface contaminants on the as-prepared Pd NCs, reliable electrochemical features were obtained and compared. These results revealed that {100} enclosed Pd nanocubes exhibit a higher catalytic ability toward FA oxidation.[120] Along this line, further improved FAO performance has been reported on {100} dominant penta-twinned Pd nanorods.[121] Additionally, Meng *et al.*[122] obtained thorn-like single crystal Pd nanoclusters composed of hexahedral units along the ⟨220⟩ direction by square wave electrodeposition, possessing a higher activity toward FAO as compared to the Pd black catalyst. On the other hand, Shao *et al.*[123] suggested that steps and defects were more active for FAO than terraces, which leads to a restricted activity on shape-selective materials as compared to conventional Pd (around 5 nm) as the former contained fewer defects and edge sites. Such a divergence thus calls for more accurate electrochemical catalysis evaluation on more ''cleaned'' nanocrystal surfaces.

3.3 Pt-based catalysts

Surface modified Pt-based catalysts. Benefited from the so called ''third-body effect'' or ''ensemble effect'', the dehydration pathway for FA oxidation and thus the CO poisoning on Pt can be impeded, leading to a significant enhancement of oxidation current and a negatively shifted peak potential. Great successes have already been reached on the state-of-the-art Pt-based catalysts by the surface modification or alloying strategies.[7]

As shown in Fig. 9, Kim *et al.*[124] studied FA oxidation on Pt black catalysts modified by irreversibly adsorbed Bi with coverages controlled from 0.05 to 0.25, and reported a Bi coverage-dependent catalytic activity. According to their results, the CO poisoning is almost completely suppressed when the Bi coverage was more than 0.18 on these electrodes, meanwhile the best catalytic performance was reached. Saez *et al.*[125] tested Bi-modified Pt electrodes with different Bi coverages in concentrated FA solutions.

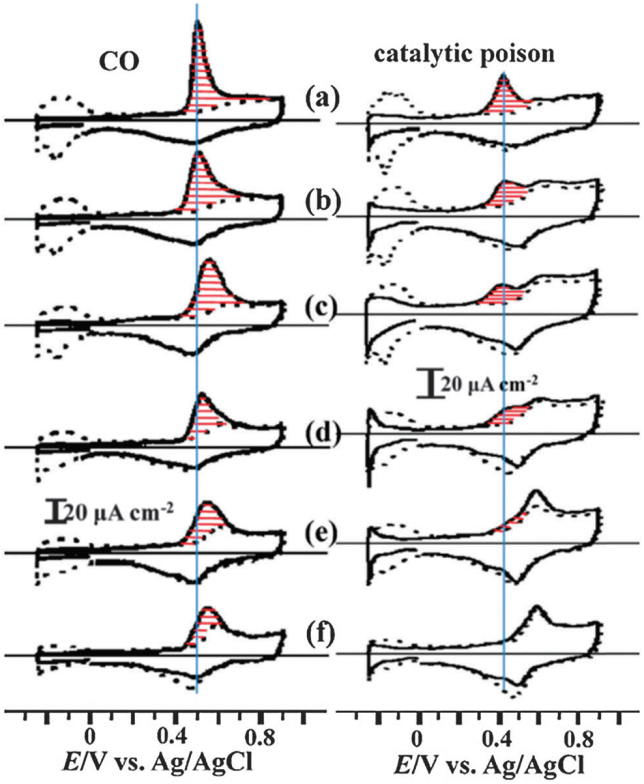

Fig. 9 Stripping voltammograms of adsorbed CO and catalytic poison species on Pt black coated electrodes modified by irreversibly adsorbed Bi with different coverages [(a) 0, (b) 0.05, (c) 0.08, (d) 0.13, (e) 0.18 and (f) 0.25] in 0.5 M H_2SO_4 solution (reproduced from ref. 124 with permission from Elsevier).

The presence of Bi caused a 4–6 fold increase of the electro-oxidation current as compared to the unmodified Pt electrodes, and the best performance was obtained with the Bi coverage of 50% in 9 M FA. On the preferential (111) oriented Pt nanoparticles,[126] the highest activity was obtained at the Bi coverage of 0.88. Such a big difference may be due to the different Bi modification methods, type of Pt electrodes and the concentration of FA solutions. Uhm *et al.*[127] modified Pt with Bi by the UPD method for practical DFAFC applications, and significantly enhanced cell performances including an impressive long-term durability was achieved with a Pt loading of only 0.5 mg cm^{-2} in an operating fuel cell.

Other III, IV or Vth group metals have also be applied as the adatoms to modify Pt catalysts. Sun's group employed the UPD strategy to fabricate either Bi[128] or Au[129] adatoms decorated tetrahexahedral Pt nanocrystals, leading to a drastically enhanced FAO in comparison with bare Pt nanocrystals. Buso-Rogero *et al.*[130] reported the promotional effect of Tl-modified Pt nanoparticles resulting in the inhibition of CO_{ads} formation and thus improving the onset potential for the complete formic acid oxidation to CO_2. Lee *et al.*[131] found the UPD Sb induced a lower onset potential of FA oxidation and doubled the power density as compared to the unmodified Pt catalyst. The fundamental understanding regarding the beneficial effect of surface modification on FAO on Pt can be utilized to synthesize efficient anode catalysts for real fuel cells. Yu *et al.*[132] chemically deposited different amounts of Pb or Sb on a commercial 40% Pt/C catalyst and compared the performances of these catalysts in a multi-anode DFAFC. The maximum catalytic activity was obtained at Pt : M (M = Pb and Sb) mass ratio of 3 : 1 for both Pt–Pb/C and Pt–Sb/C. The same group extended this multi-anode approach to make the comparison of co-deposited PdM/C (M = Bi, Mo, or V) catalysts and Pb or Sn decorated Pt/C catalysts with commercial Pd/C, PtRu/C, and Pt/C catalysts, aiming at improving the activity of Pt-based catalysts or the stability of Pd-based catalysts.[133] Notably in their multi-anode fuel cell screening tests (shown in Fig. 10), PtPb/C and PtSn/C catalysts showed significantly higher activities than the commercial Pt/C catalyst, while the PdBi/C exhibited a higher stability than the commercial Pd/C catalyst. In order to overcome the complexity of the conventional UPD method that requires the external potential control, a more facile electroless mimetic underpotential deposition (MUPD) approach was proposed to realize the submonolayer deposition of Sb or Pb on Pt surfaces.[134,135] The MUPD method is an all-wet chemical immersion process which involves selecting reasonable reductants to adjust the open circuit potential of a metallic substrate to a suitable UPD potential for the second metal deposition. Compared to UPD, this approach is much easier for scale-up surface modification of various types of catalysts, in particular, the existing nanocatalysts in powder form.

Another type of high performance FA oxidation catalysts is obtained by decorating Pt on other metal surfaces. Kristian *et al.*[136] deposited submonolayer of Pt on Au nanoparticles and found markedly improved catalytic activity for FA direct oxidation and suppression of CO_{ad} poison formation. They further screened the Pt : Au mole ratio ranging from 1 : 10 to 1 : 2 and concluded that the specific activity of PtAu/C with a Pt/Au mole ratio of 1 : 8 was the best.[137]

Pt-based alloy nanocatalysts. Other than the surface modified Pt catalysts, Pt based alloy catalysts were also intensively studied over the past several years. The alloy component includes but is not limited to Au, Bi, Pb, Sb, Pd, Ru, Sn, Cu, Ag and Fe. Chen *et al.*[76] prepared a series of Pt–Au/C bimetallic nanocatalysts for FA electro-oxidation to establish the correlation between the bimetallic composition and the electrocatalytic activity. The $Pt_{50}Au_{50}$/C shows the highest performance with a mass-specific activity eight times higher than that of Pt/C. Such an optimal molar ratio for Pt:Au was also confirmed by other groups on Pt–Au nanocatalysts supported on either carbon black,[73–75] carbon nanofibers[138] or carbon nanotubes.[139] Furthermore, the randomly arranged PtPb[140] and Pt_3Pb,[141] the intermetallic PtPb alloy,[142,143] and the PtBi alloy with low amounts of Bi (Pt : Bi molar ratio is 11 : 1)[144] were also reported to exhibit enhanced catalytic activity and excellent CO tolerance for FA oxidation.

Pt–Ru and Pt–Sn alloy catalysts have been recognized as the most effective anode catalysts for direct methanol fuel cells.[145,146] They show good catalytic activities for FA oxidation as well. Chen *et al.*[147] prepared and screened a series of carbon-supported bimetallic Pt–Ru catalysts with a high degree of alloying and different Pt/Ru atomic ratios for FA oxidation and demonstrated the importance of these two factors in the catalytic performance.

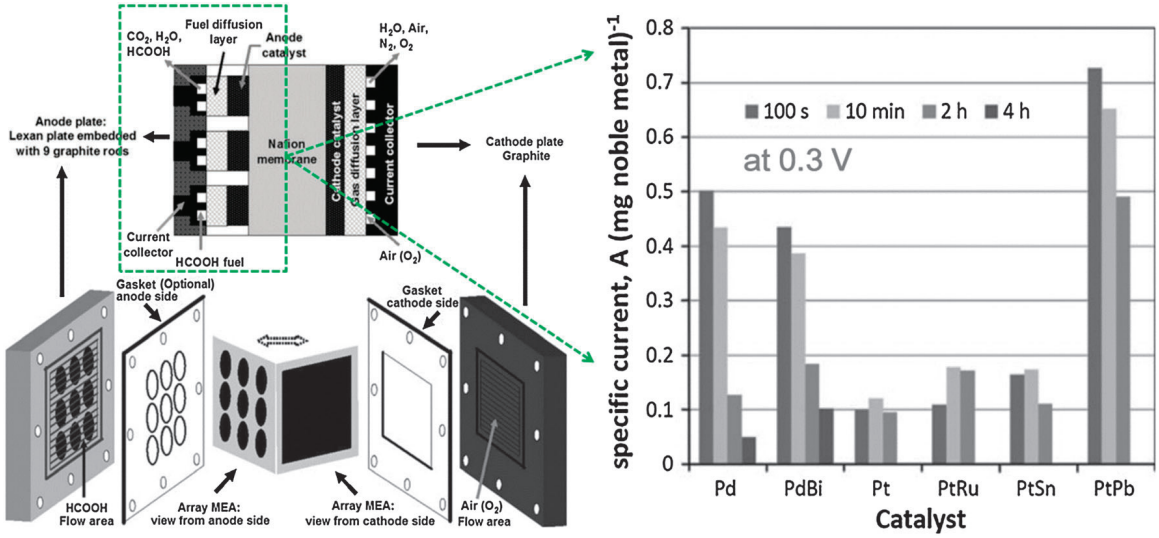

Fig. 10 Electrocatalytic performance screening of Pd–M and Pt–M catalysts in a multi-anode direct formic acid fuel cell (reproduced from ref. 133 with permission from Springer).

The effectiveness of adding Ru to Pt catalysts for enhancing FAO was also examined on the Pt–Ru alloys with different nanostructures[148,149] or synthesis methods.[150,151] In addition, Ag,[77,152] Fe[78,79] and Cu[80,153] were also shown as promising candidates to prepare Pt-based alloy catalysts for FA oxidation. Notably, the less noble component such as Cu[80] could be dealloyed intentionally to form a Pt enriched skin structure that may further benefit the FA oxidation.

3.4 Other morphological controls of the nanocatalysts

The aforementioned approaches to synthesize the Pt- and Pd-based catalysts mainly focus on tailoring the catalytic properties by tuning the electronic structure and the surface atomic arrangement. Besides the shape, other morphological factors including the size, dispersion and hollow or core–shell structure play also a significant role in enhancing FAO catalytic activity and durability. In the following, we summarized efforts made in this direction.

Mazumder *et al.*[154,155] reported a facile synthesis method to prepare 4.5 nm Pd nanocatalysts with a fairly good size dispersion (Fig. 11a) through the reduction of $Pd(acac)_2$ with oleylamine and borane tributylamine complex as the stabilizers. These Pd nanocatalysts subsequently cleaned with acetic acid to remove the surface capping agents showed an attractive durability for FAO with no obvious degradation even after 1500 voltammetric cycles under ambient conditions (Fig. 11b–d). Obviously, the uniform size distribution of the nanocatalysts provides much better resistance to the so-called ''Ostwald Ripening'' or metal dissolution during the FA oxidation and thus enhances the durability.

In contrast to the preparation approaches using organic solvents,[154,156] the impregnation methods in aqueous solutions may be more favorable because of the easy removal of surface organic residues. Zhang *et al.*[157] reported the preparation of Pd/C catalysts with NH_4F and H_3BO_3 as the stabilizers, and demonstrated

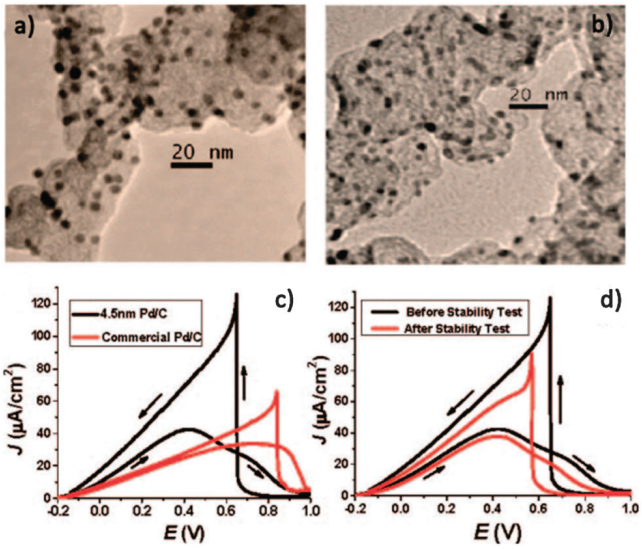

Fig. 11 TEM images of 4.5 nm Pd/C catalyst before (a) and after the stability test (b). (c) Specific activity of FA oxidation of the catalyst shown in (a) and the commercial Pd/C catalyst. (d) Specific activity of FAO of the 4.5 nm Pd/C before and after the stability test (reprinted with permission from ref. 154. Copyright 2009, American Chemical Society).

the effectiveness of applying EDTA as the capping agent and a thermal annealing treatment at 120 °C for achieving a better catalytic activity.[158] Similarly, Wang *et al.*[159] synthesized ultrafine 2.1 nm Pd/C with uniform size by using CyDTA as an alternative capping agent. Moreover, stabilizing agent-free methods[160,161] using NH_3 as the complex and $NaBH_4$ as the reducing agent have been used to prepare Pd/C catalysts.

Hollow structures have a very high surface to bulk atomic ratio and can effectively increase the catalyst mass activity. Ge *et al.*[162] reported a controllable synthesis method to prepare either hollow nanospheres or solid nanoparticles with the solution pH below 9 or higher than 10, respectively, by using

Co nanoparticles as a sacrificial template. These nanostructures showed enhanced catalytic activity towards FA oxidation. Co nanoparticles were applied to prepare a polypyrrole-modified carbon-supported Pd hollow catalysts for FA oxidation as well.[163] Similar galvanic replacement reaction was also employed to synthesize Pd–Pb/C hollow nanospheres with a larger electrochemical active surface area.[164] Ag@Pd core–shell nanotubes were prepared from a galvanic replacement reaction between Ag nanowires and a Pd(II) precursor solution.[165] The increase of the number of surface active Pd sites and the modified Pd electronic structure by Ag were proposed to be responsible for the improvement of electrocatalytic activity and durability for FA oxidation.

Despite the above successes, one concern is the surface cleanness of these as-prepared nanocatalysts. Organic solvents and various surfactants with strong specific interaction with the catalysts are used to control the size and dispersion of the catalyst particles. Despite the post-synthesis cleaning, some of these species remain adsorbed on the catalyst surfaces. In most cases, the impact of these organic solvents and surfactants on the catalytic activity is largely ignored. We believe that more attention needs to be paid to the surface cleanness, because the relevant electrochemical processes may be extremely sensitive to the surface contaminations. The influence of the residual surfactants on the catalytic activity has recently been reported.[166] A future challenge would be developing methods to obtain clean catalyst surfaces so that the intrinsic activity of the catalysts can be reliably obtained.

3.5 Catalyst supports

As substitutes to the normally used Vulcan XC-72® carbon black, ordered mesoporous carbon (OMC), carbon nanotubes (MWCNTs), graphene and graphene oxide (GO) have been employed as supports of nanocatalysts for FA oxidation because of their large surface area, good thermal and chemical stability as well as great electrical conductivity.

One of the largest obstacles to apply these novel supports is the inefficient binding sites on the innate materials. Great efforts have been put on the development of proper pretreatments to functionalize the supports for better attachment of the metal nanoparticles. Nazar *et al.*[167] introduced an effective sulfur-coating strategy onto OMC to trap the metal precursors, leading to a high dispersion of Pt/Pd-based nanocrystallites as well as a tunable size control from 1.5 nm to 3 nm. They also point out that 3 nm intermetallic Pt–Bi nanocrystals embedded in OMC-S exhibits the best electrocatalytic FAO performance among their tested samples. Bai *et al.*[168] reported a novel method to functionalize MWCNTs with 1,10-phenanthroline (phen-MWCNTs) to immobilize Pd nanoparticles, which preserves the integrity and electronic structure of MWCNTs and meanwhile provides highly effective functional groups on the MWCNT surfaces (shown in Fig. 12). Yang *et al.*[169] prepared Pd catalysts supported on MWCNTs pretreated in a mixture of sulfuric and 4-aminobenzene sulfonic acid, and demonstrated an enhanced FAO activity due to the improved water-solubility and dispersion of MWCNTs. Zheng *et al.*[170] recently synthesized highly dispersed Pd catalysts on phosphonate

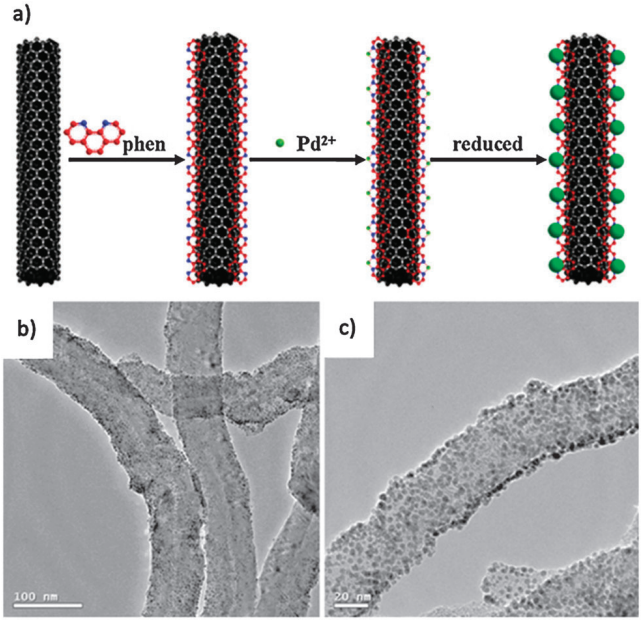

Fig. 12 (a) Scheme of the formation mechanism of the Pd/phen-MWCNT catalyst. (b, c) TEM images of the synthesized Pd/phen-MWCNT catalysts (reproduced from ref. 167 with permission from Elsevier).

functionalized MWCNTs, leading to an enhanced FAO performance than the un-phosphonated counterpart. Moreover, the immobilization of metal nanoparticles on CNT has been realized by conducting the synthesis in glutamate solutions,[171] or by a simple two-stage polyol method[172] followed by H_2–Ar annealing.[173]

In recent years, graphene has received increasing attention as 2D supports for loading metal nanocatalysts in fuel cell applications due to its extremely high surface area ($\sim$2600 $m^2\ g^{-1}$) and high electrical conductivity (10^5–10^6 S m^{-1}).[174,175] Rao *et al.*[176] prepared graphene-supported Pt–Au alloy nanoparticles by an ethylene glycol reduction method. The high electrocatalytic performance of the as-prepared Pt–Au/graphene was attributed to the intrinsic high degree of graphitization of graphene and the enhanced metal–support interaction. Bong *et al.*[177] synthesized 80 wt% Pd/graphene nanosheet with good dispersion by a colloidal method using potassium triethylborohydride as a reducing agent and tetraoctylammonium bromide $N(Oct)_4Br$ as a surfactant in THF solutions. Yang *et al.*[178] supported Pd nanoparticles on graphene nanosheet–MWCNT composites by a microwave-assisted polyol process. The optimal electrocatalytic activity and stability for FA oxidation was achieved when the mass ratio of GO to MWCNTs is 5 : 1.

So far, great achievements have been attained in the past few years in the design and development of efficient Pd and Pt-based nanocatalysts toward FA oxidation by tuning their electronic structure, surface atomic arrangements, geometric structure as well as catalyst supports. However, there are plenty of rooms for further improvement of these catalysts in terms of increasing the durability and lowering the noble metal content for practical fuel cell applications.

4. Progress in practical DFAFCs

As stated in the outset, DFAFCs are promising alternative power sources. They possess a higher electromotive force (EMF = 1.45 V) than the more commonly discussed direct methanol fuel cells (DMFCs, EMF = 1.21 V) and hydrogen fuel cells (EMF = 1.23 V). In addition, formic acid is more convenient to store than H_2 gas. As compared to DMFCs, though the theoretical volume energy density of formic acid (1725 W h L^{-1}) is *ca.* 1/3 of that for methanol (4780 W h L^{-1}), the fuel crossover flux through the proton exchange membrane is much smaller in DFAFCs. Thus they can be operated at a much higher concentration of 10 to 15 M and provide a practically higher output cell energy density, considering that 1–3 M methanol is usually used in DMFCs. Furthermore, in contrast to the sluggish methanol oxidation kinetics, the FA oxidation is quite facile, leading to a much higher practical output power. Nevertheless, the performance of practical DFAFCs with Pt or Pt–Ru[179] catalysts in earlier studies was not as satisfactory as the H_2–O_2 PEM fuel cells, until Masel's group[180,181] reported a maximum power density of 248–336 mW cm^{-2} at 22 °C with Pd black as the anode catalyst and 3–12 M FA as the fuel. They also demonstrated a passive miniature air breathing DFAFC with 2 cm × 2.4 cm × 1.4 cm in size producing a power density up to 33 mW cm^{-2} under ambient conditions.[51]

As mentioned in the above sections, the mechanistic study of FAO on Pd and Pt surfaces may shed light on the rational synthesis of novel and efficient Pd- and Pt-based electrocatalysts, and thus push forward the practical progress of DFAFCs. Most recently, by applying carbon supported Pd–Ni_2P as the anode catalysts, Chang *et al.*[182] reported the DFAFCs with a maximum power density of 550 mW cm^{-2} with 3 M FA at 30 °C. Furthermore, a 30 W DFAFC hybrid power system for a laptop computer was also developed, which can operate under a substantial computing load for 2.5 h using only a 280 mL tank of 50 wt% FA fuel.[179] In order to achieve a higher utilization of noble metal catalyst and an easier accessibility of both reactants and electrons to active sites, Wang *et al.* developed a ultra-thin layer structured anode consisting of one atomic layer Pt[183] or Bi@Pt[184] supported on nanoporous gold (NPG), see Fig. 13. They also prepared a DFAFC stack with 10 unit cells (each cell has an area of 6 × 8 cm^2) using NPG–Pt–Bi catalysts as anodes and Pt/C as cathodes, and achieved a maximum power density of 40.9 W at a current of 12.9 A together with little voltage variation for each individual cell around 0.5 V.[184] Successes were also achieved in the design and fabrication of medium-scale DFAFC stacks to act as the power sources of portable devices.[185] Liao's group have done a series of work on the improvement of fuel cell structures for the miniature DFAFCs, including the air breathing compact cell,[186] twin-cell[187] and 4-cell stack structures,[188] among which a maximum power density of 56.6 mW cm^{-2} was achieved for a 4-cell stack.

Notably, to address the power supply to a microfluidic chip, membrane-free microfluidic fuel cells have been developed, which exploit the laminar flow that occurs in liquids flowing at low Reynolds number (Re) to eliminate convective mixing of anodic and cathodic fuels.[189,190] Recently, Ma *et al.* reported a formic acid microfluidic fuel cell system with anode and cathode electrodes made from Pd/C and Pt/MWCNT catalysts, and a maximum power density of 23 mW cm^{-2} with 5 M HCOOH

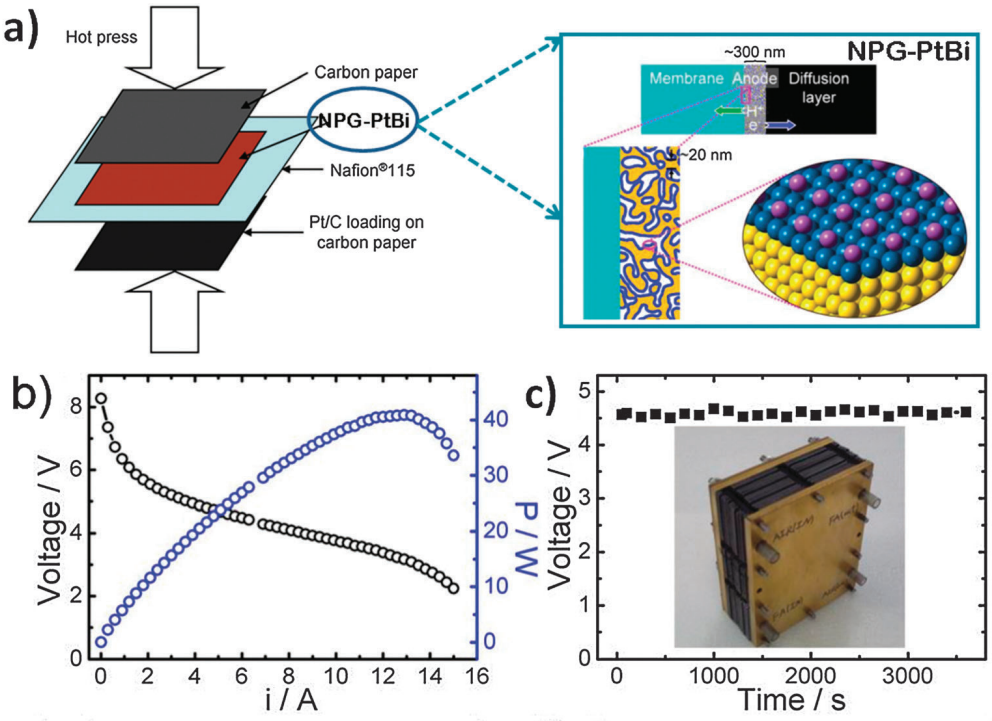

Fig. 13 (a) Schematic illustration of membrane electrode assembly structures of nanoporous gold supported PtBi (NPG-PtBi) catalysts and (b, c) the corresponding 10-cell stack performance recorded at room temperature, with 3 M FA as the fuel (10 mL min^{-1} flow) and dry air as the oxidant (2 L min^{-1} flow). Reproduced from ref. 183 with permission from The Royal Society of Chemistry and ref. 184 with permission from Springer.

as the fuel was achieved.[191] Zhu *et al.* demonstrated an air-breathing microfluidic fuel cell with an array of graphite cylinder anodes with a Pd catalyst, leading to confined CO_2 bubbles within the anode arrays which are removed periodically.[192]

Some other efforts have been made to further raise the power density and prolong the durability of the practical DFAFCs by optimizing the FA concentrations,[193] catalysts layer structures[194–198] as well as the Nafion membrane preparation methods.[199–201] Baik *et al.*[202] investigated the performance of DFAFCs consisting of membrane electrode assembly (MEA) prepared by different catalyst coating methods. As compared to the direct painting and air spraying, the MEAs made by a dual mode spraying method showed the best performance as high as 240 mW cm^{-2} at 5 M FA, mainly owing to the uniform particle distribution and the small particle size of the catalysts prepared through this method. The effects of mass transport and conductivity of the catalyst layer[203] on DFAFC performance were also studied with PtRu/C as the anode catalyst. The increase of cell resistance caused by the membrane dehydration was pointed out as the most responsible for decreasing the overall cell performance and the plain carbon paper was suggested as the support to load catalysts to facilitate such mass transport. Besides, Cai *et al.*[204] reported the MEA fabrication by decal method instead of traditional hot pressing can result in a better triple phase boundary and a lower FA crossover.

In terms of the influence of Nafion, Kang *et al.*[199] found that Nafion ionomer aggregation within the anode catalytic layer plays an important role on the utilization of the catalysts through the XPS and EIS investigations. They proposed that a simple heat pretreatment method[200] may decrease the particle size of Nafion ionomers and congregation formed from Nafion ionomer and Pd nanoparticles, hence enhance the DFAFC performance. Morgan *et al.*[201] suggested that a DFAFC with the anode loading of 30 wt% Nafion showed the best stability among three different Nafion loadings, which showed the minimum loss of the electrochemical active surface area of the catalyst after 600 potential cycles between 0.02 V and 1.2 V (*vs.* RHE).

5. Concluding remarks and outlook

Thanks to a deeper mechanistic understanding of formic acid oxidation on Pt and Pd surfaces brought about by the fundamental studies with spectroscopic, single crystal and computational techniques, various high-performance Pt and Pd-based nanocatalysts have been attained using the "synthesis-by-design" concept by subtle control of the electronic and geometric structures of metal nanoparticles as well as the catalyst supports. Progresses have also been made in the development of miniature direct formic acid fuel cells and the corresponding operation conditions.

Despite these successes, many opportunities and challenges remain for future investigations in either the fundamental and practical aspects. In our humble opinion, the following key issues are to be addressed: (1) further understanding on the reaction mechanism, especially the chemical nature of the reactive intermediate of formic acid oxidation and its adsorption mode on Pt and Pd electrodes; (2) the relationship between the binding energy of the reactive intermediate and the corresponding formic acid oxidation activity; (3) tailoring the selectivity and activity of electrocatalysis of formic acid oxidation by manipulating electronic and geometric structures; (4) synthesis of nanocatalysts with multi-components and defined facet orientations; (5) studying structural stability and evolution of nanocatalysts during the electrochemical process and (6) development of practical direct formic acid fuel cells with full utilization of nanocatalysts by optimizing the membrane electrode assembly design. Along with the investigation of aforementioned problems, we also believe that the boom in research methodology including *in situ* spectroscopies and density functional theory calculations would promote the developments in electrocatalysis and proton exchange membrane fuel cells.

Acknowledgements

This work is supported by the NSFC (No. 21273046, 21327901 and 21073045) and SMCST (No. 11JC140200). Partial support from NSF (CHE-1156425) to S.Z. is also acknowledged.

References

1 A. Capon and R. Parsons, *J. Electroanal. Chem.*, 1973, **44**, 1–7.
2 A. Capon and R. Parsons, *J. Electroanal. Chem.*, 1973, **45**, 205–231.
3 A. Capon and R. Parsons, *J. Electroanal. Chem.*, 1973, **44**, 239–254.
4 X. Wang, J. M. Hu and I. M. Hsing, *J. Electroanal. Chem.*, 2004, **562**, 73–80.
5 K. J. Jeong, C. A. Miesse, J. H. Choi, J. Lee, J. Han, S. P. Yoon, S. W. Nam, T. H. Lim and T. G. Lee, *J. Power Sources*, 2007, **168**, 119–125.
6 P. G. Pickup and X. W. Yu, *J. Power Sources*, 2008, **182**, 124–132.
7 S. Uhm, H. J. Lee and J. Lee, *Phys. Chem. Chem. Phys.*, 2009, **11**, 9326–9336.
8 N. V. Rees and R. G. Compton, *J. Solid State Electrochem.*, 2011, **15**, 2095–2100.
9 H. Li, J. Shen, G. Yang, Y. Tang and T. Lu, *Chem. Res. Chin. Univ.*, 2011, **32**, 1445–1450.
10 M. Grasemann and G. Laurenczy, *Energy Environ. Sci.*, 2012, **5**, 8171–8181.
11 J. Lipkowski and P. N. Ross, *Electrocatalysis*, Wiley-VCH, New York, 1998.
12 S. G. Sun, J. Clavilier and A. Bewick, *J. Electroanal. Chem.*, 1988, **240**, 147–159.
13 A. Miki, S. Ye and M. Osawa, *Chem. Commun.*, 2002, 1500–1501.
14 H. Miyake, T. Okada, G. Samjeske and M. Osawa, *Phys. Chem. Chem. Phys.*, 2008, **10**, 3662–3669.
15 G. Samjeske and M. Osawa, *Angew. Chem., Int. Ed.*, 2005, **44**, 5694–5698.
16 G. Samjeske, A. Miki, S. Ye and M. Osawa, *J. Phys. Chem. B*, 2006, **110**, 16559–16566.

17 M. Osawa, K. Komatsu, G. Samjeske, T. Uchida, T. Ikeshoji, A. Cuesta and C. Gutierrez, *Angew. Chem., Int. Ed.*, 2011, **50**, 1159–1163.

18 A. Cuesta, G. Cabello, C. Gutierrez and M. Osawa, *Phys. Chem. Chem. Phys.*, 2011, **13**, 20091–20095.

19 A. Cuesta, G. Cabello, M. Osawa and C. Gutierrez, *ACS Catal.*, 2012, **2**, 728–738.

20 V. Grozovski, F. J. Vidal-Iglesias, E. Herrero and J. M. Feliu, *ChemPhysChem*, 2011, **12**, 1641–1644.

21 Y. X. Chen, M. Heinen, Z. Jusys and R. J. Behm, *Angew. Chem., Int. Ed.*, 2006, **45**, 981–985.

22 Y. X. Chen, M. Heinen, Z. Jusys and R. J. Behm, *Langmuir*, 2006, **22**, 10399–10408.

23 Y. X. Chen, S. Ye, M. Heinen, Z. Jusys, M. Osawa and R. J. Behm, *J. Phys. Chem. B*, 2006, **110**, 9534–9544.

24 Y. X. Chen, M. Heinen, Z. Jusys and R. J. Behm, *ChemPhysChem*, 2007, **8**, 380–385.

25 J. Xu, D. F. Yuan, F. Yang, D. Mei, Z. B. Zhang and Y. X. Chen, *Phys. Chem. Chem. Phys.*, 2013, **15**, 4367–4376.

26 H. Okamoto, Y. Numata, T. Gojuki and Y. Mukouyama, *Electrochim. Acta*, 2014, **116**, 263–270.

27 M. Neurock, M. Janik and A. Wieckowski, *Faraday Discuss.*, 2008, **140**, 363–378.

28 H. F. Wang and Z. P. Liu, *J. Phys. Chem. C*, 2009, **113**, 17502–17508.

29 W. Gao, J. A. Keith, J. Anton and T. Jacob, *J. Am. Chem. Soc.*, 2010, **132**, 18377–18385.

30 W. Gao, J. E. Mueller, Q. Jiang and T. Jacob, *Angew. Chem., Int. Ed.*, 2012, **51**, 9448–9452.

31 J. Joo, T. Uchida, A. Cuesta, M. T. M. Koper and M. Osawa, *J. Am. Chem. Soc.*, 2013, **135**, 9991–9994.

32 J. Joo, T. Uchida, A. Cuesta, M. T. M. Koper and M. Osawa, *Electrochim. Acta*, 2014, **129**, 127–136.

33 M. T. M. Koper, *Chem. Sci.*, 2013, **4**, 2710–2723.

34 D. Mei, Z. D. He, D. C. Jiang, J. Cai and Y. X. Chen, *J. Phys. Chem. C*, 2014, **118**, 6335–6343.

35 E. Herrero, presented in part at the 225th ECS Meeting (May 11-15, 2014), Orlando, USA, 2014.

36 J. V. Perales-Rondón, E. Herrero and J. M. Feliu, *Electrochim. Acta*, 2014, DOI: 10.1016/j.electacta.2014.06.057.

37 S. Brimaud, J. Solla-Gullón, I. Weber, J. M. Feliu and R. J. Behm, *ChemElectroChem*, 2014, **1**, 1075–1083.

38 K. Jiang, K. Xu, S. Zou and W.-B. Cai, *J. Am. Chem. Soc.*, 2014, **136**, 4861–4864.

39 C. Lamy, J. M. Leger, J. Clavilier and R. Parsons, *J. Electroanal. Chem.*, 1983, **150**, 71–77.

40 K. Kunimatsu and H. Kita, *J. Electroanal. Chem.*, 1987, **218**, 155–172.

41 N. M. Markovic and P. N. Ross, *Surf. Sci. Rep.*, 2002, **45**, 117–229.

42 C. T. Campbell, J. M. Campbell, P. J. Dalton, F. C. Henn, J. A. Rodriguez and S. G. Seimanides, *J. Phys. Chem.*, 1989, **93**, 806–814.

43 A. Cuesta, M. Escudero, B. Lanova and H. Baltruschat, *Langmuir*, 2009, **25**, 6500–6507.

44 Y. Y. Yang, Q. H. Wu, Z. Y. Zhou, M. S. Zheng, S. P. Chen and S. G. Sun, *Spectrosc. Spect. Anal.*, 2000, **20**, 765–767.

45 Y. Y. Yang, Z. Y. Zhou and S. G. Sun, *J. Electroanal. Chem.*, 2001, **500**, 233–240.

46 S.-C. Chang, Y. Ho and M. J. Weaver, *Surf. Sci.*, 1992, **265**, 81–94.

47 V. Grozovski, V. Climent, E. Herrero and J. M. Feliu, *Phys. Chem. Chem. Phys.*, 2010, **12**, 8822–8831.

48 B. Peng, H. F. Wang, Z. P. Liu and W. B. Cai, *J. Phys. Chem. C*, 2010, **114**, 3102–3107.

49 R. Wang, C. Wang, W.-B. Cai and Y. Ding, *Adv. Mater.*, 2010, **22**, 1845–1848.

50 R. G. Zhang, H. Y. Liu, B. J. Wang and L. X. Ling, *J. Phys. Chem. C*, 2012, **116**, 22266–22280.

51 S. Ha, B. Adams and R. I. Masel, *J. Power Sources*, 2004, **128**, 119–124.

52 W. S. Jung, J. H. Han and S. Ha, *J. Power Sources*, 2007, **173**, 53–59.

53 A. Mikolajczuk, A. Borodzinski, P. Kedzierzawski, L. Stobinski, B. Mierzwa and R. Dziura, *Appl. Surf. Sci.*, 2011, **257**, 8211–8214.

54 V. Solis, T. Iwasita, A. Pavese and W. Vielstich, *J. Electroanal. Chem.*, 1988, **255**, 155–162.

55 S. Uhm, S. T. Chung and J. Lee, *J. Power Sources*, 2008, **178**, 34–43.

56 W. Zhou and J. Y. Lee, *J. Phys. Chem. C*, 2008, **112**, 3789–3793.

57 X. Yu and P. G. Pickup, *Electrochem. Commun.*, 2009, **11**, 2012–2014.

58 M. J. Ren, Y. Y. Kang, W. He, Z. Q. Zou, X. Z. Xue, D. L. Akins, H. Yang and S. L. Feng, *Appl. Catal., B*, 2011, **104**, 49–53.

59 Y. M. Zhu, Z. Khan and R. I. Masel, *J. Power Sources*, 2005, **139**, 15–20.

60 Y. Zhou, J. G. Liu, J. L. Ye, Z. G. Zou, J. H. Ye, J. Gu, T. Yu and A. D. Yang, *Electrochim. Acta*, 2010, **55**, 5024–5027.

61 M. Arenz, V. Stamenkovic, T. J. Schmidt, K. Wandelt, P. N. Ross and N. M. Markovic, *Phys. Chem. Chem. Phys.*, 2003, **5**, 4242–4251.

62 S. Pronkin, M. Hara and T. Wandlowski, *Russ. J. Electrochem.*, 2006, **42**, 1177–1192.

63 K. Brandt, M. Steinhausen and K. Wandelt, *J. Electroanal. Chem.*, 2008, **616**, 27–37.

64 J. Y. Wang, H. X. Zhang, K. Jiang and W. B. Cai, *J. Am. Chem. Soc.*, 2011, **133**, 14876–14879.

65 M. D. Obradovic and S. L. Gojkovic, *Electrochim. Acta*, 2013, **88**, 384–389.

66 H. X. Zhang, S. H. Wang, K. Jiang, T. Andre and W. B. Cai, *J. Power Sources*, 2012, **199**, 165–169.

67 W. J. Zhou and J. Y. Lee, *J. Phys. Chem. C*, 2008, **112**, 3789–3793.

68 M. Watanabe, Y. Furuuchi and S. Motoo, *J. Electroanal. Chem.*, 1985, **191**, 367–375.

69 M. Watanabe, M. Horiuchi and S. Motoo, *J. Electroanal. Chem.*, 1988, **250**, 117–125.

70 M. Shibata, N. Furuya, M. Watanabe and S. Motoo, *J. Electroanal. Chem.*, 1989, **263**, 97–108.

71 A. Boronat-González, E. Herrero and J. M. Feliu, *J. Solid State Electrochem.*, 2013, 1–13.
72 F. J. Vidal-Iglesias, A. Lopez-Cudero, J. Solla-Gullon and J. M. Feliu, *Angew. Chem., Int. Ed.*, 2013, **52**, 964–967.
73 J. B. Xu, T. S. Zhao and Z. X. Liang, *J. Power Sources*, 2008, **185**, 857–861.
74 M. D. Obradovic, A. V. Tripkovic and S. L. Gojkovic, *Electrochim. Acta*, 2009, **55**, 204–209.
75 S. Zhang, Y. Y. Shao, G. P. Yin and Y. H. Lin, *Angew. Chem., Int. Ed.*, 2010, **49**, 2211–2214.
76 G. Q. Chen, Y. H. Li, D. Wang, L. Zheng, G. R. You, C. J. Zhong, L. F. Yang, F. Cai, J. X. Cai and B. H. Chen, *J. Power Sources*, 2011, **196**, 8323–8330.
77 J. B. Xu, T. S. Zhao and Z. X. Liang, *J. Phys. Chem. C*, 2008, **112**, 17362–17367.
78 W. Chen, J. Kim, S. H. Sun and S. W. Chen, *Phys. Chem. Chem. Phys.*, 2006, **8**, 2779–2786.
79 W. Chen, J. M. Kim, L. P. Xu, S. H. Sun and S. W. Chen, *J. Phys. Chem. C*, 2007, **111**, 13452–13459.
80 H. Z. Yang, L. Dai, D. Xu, J. Y. Fang and S. Z. Zou, *Electrochim. Acta*, 2010, **55**, 8000–8004.
81 T. Bligaard and J. K. Nørskov, *Electrochim. Acta*, 2007, **52**, 5512–5516.
82 U. B. Demirci, *J. Power Sources*, 2007, **173**, 11–18.
83 A. Ruban, B. Hammer, P. Stoltze, H. L. Skriver and J. K. Nørskov, *J. Mol. Catal. A: Chem.*, 1997, **115**, 421–429.
84 B. Hammer and J. K. Nørskov, *Adv. Catal.*, 2000, **45**, 71–129.
85 J. Greeley, J. K. Nørskov and M. Mavrikakis, *Annu. Rev. Phys. Chem.*, 2002, **53**, 319–348.
86 M. Mavrikakis, B. Hammer and J. K. Nørskov, *Phys. Rev. Lett.*, 1998, **81**, 2819–2822.
87 L. A. Kibler, A. M. El-Aziz, R. Hoyer and D. M. Kolb, *Angew. Chem., Int. Ed.*, 2005, **44**, 2080–2084.
88 M. Wakisaka, S. Mitsui, Y. Hirose, K. Kawashima, H. Uchida and M. Watanabe, *J. Phys. Chem. B*, 2006, **110**, 23489–23496.
89 J. Solla-Gullon, F. J. Vidal-Iglesias and J. M. Feliu, *Annu. Rep. Prog. Chem., Sect. C: Phys. Chem.*, 2011, **107**, 263–297.
90 S. C. Chang, L. W. H. Leung and M. J. Weaver, *J. Phys. Chem.*, 1990, **94**, 6013–6021.
91 T. Iwasita, X. Xia, E. Herrero and H.-D. Liess, *Langmuir*, 1996, **12**, 4260–4265.
92 N. Hoshi, K. Kida, M. Nakamura, M. Nakada and K. Osada, *J. Phys. Chem. B*, 2006, **110**, 12480–12484.
93 N. Hoshi, M. Nakamura and K. Kida, *Electrochem. Commun.*, 2007, **9**, 279–282.
94 R. Larsen, S. Ha, J. Zakzeski and R. I. Masel, *J. Power Sources*, 2006, **157**, 78–84.
95 R. F. Wang, S. J. Liao and S. Ji, *J. Power Sources*, 2008, **180**, 205–208.
96 X. M. Wang and Y. Y. Xia, *Electrochem. Commun.*, 2008, **10**, 1644–1646.
97 Z. L. Liu and X. H. Zhang, *Electrochem. Commun.*, 2009, **11**, 1667–1670.
98 Z. H. Zhang, J. J. Ge, L. A. Ma, J. H. Liao, T. H. Lu and W. Xing, *Fuel Cells*, 2009, **9**, 114–120.
99 Y. Liu, L. W. Wang, G. Wang, C. Deng, B. Wu and Y. Gao, *J. Phys. Chem. C*, 2010, **114**, 21417–21422.
100 Q. Yuan, Z. Y. Zhou, J. Zhuang and X. Wang, *Chem. Commun.*, 2010, **46**, 1491–1493.
101 H. X. Zhang, C. Wang, J. Y. Wang, J. J. Zhai and W. B. Cai, *J. Phys. Chem. C*, 2010, **114**, 6446–6451.
102 L. Dai and S. Zou, *J. Power Sources*, 2011, **196**, 9369–9372.
103 P. P. Fang, S. Duan, X. D. Lin, J. R. Anema, J. F. Li, O. Buriez, Y. Ding, F. R. Fan, D. Y. Wu, B. Ren, Z. L. Wang, C. Amatore and Z. Q. Tian, *Chem. Sci.*, 2011, **2**, 531–539.
104 Y. G. Suo and I. M. Hsing, *Electrochim. Acta*, 2011, **56**, 2174–2183.
105 X. M. Wang, M. E. Wang, D. D. Zhou and Y. Y. Xia, *Phys. Chem. Chem. Phys.*, 2011, **13**, 13594–13597.
106 Y.-J. Deng, N. Tian, Z.-Y. Zhou, R. Huang, Z.-L. Liu, J. Xiao and S.-G. Sun, *Chem. Sci.*, 2012, **3**, 1157–1161.
107 L. Lu, L. P. Shen, Y. Shi, T. T. Chen, G. Q. Jiang, C. W. Ge, Y. W. Tang, Y. Chen and T. H. Lu, *Electrochim. Acta*, 2012, **85**, 187–194.
108 C. Wang, F. F. Shi, J. Y. Wang, H. X. Zhang and W. B. Cai, *J. Electrochem.*, 2009, **15**, 377–382.
109 R. Li, Z. Wei, T. Huang and A. Yu, *Electrochim. Acta*, 2011, **56**, 6860–6865.
110 G. J. Zhang, Y. E. Wang, X. Wang, Y. Chen, Y. M. Zhou, Y. W. Tang, L. D. Lu, J. C. Bao and T. H. Lu, *Appl. Catal., B*, 2011, **102**, 614–619.
111 G. Chen, M. Liao, B. Yu, Y. Li, D. Wang, G. You, C.-J. Zhong and B. H. Chen, *Int. J. Hydrogen Energy*, 2012, **37**, 9959–9966.
112 K. Jiang and W. B. Cai, *Appl. Catal., B*, 2014, **147**, 185–192.
113 L. L. Zhang, Y. W. Tang, J. C. Bao, T. H. Lu and C. Li, *J. Power Sources*, 2006, **162**, 177–179.
114 G. Yang, Y. Chen, Y. Zhou, Y. Tang and T. Lu, *Electrochem. Commun.*, 2010, **12**, 492–495.
115 J. Y. Wang, Y. Y. Kang, H. Yang and W. B. Cai, *J. Phys. Chem. C*, 2009, **113**, 8366–8372.
116 J. L. Haan, K. M. Stafford and R. I. Masel, *J. Phys. Chem. C*, 2010, **114**, 11665–11672.
117 J. L. Haan, K. M. Stafford, R. D. Morgan and R. I. Masel, *Electrochim. Acta*, 2010, **55**, 2477–2481.
118 M. Jin, H. Zhang, Z. Xie and Y. Xia, *Energy Environ. Sci.*, 2012, **5**, 6352–6357.
119 H.-X. Zhang, H. Wang, Y.-S. Re and W.-B. Cai, *Chem. Commun.*, 2012, **48**, 8362–8364.
120 F. J. Vidal-Iglesias, R. M. Aran-Ais, J. Solla-Gullon, E. Garnier, E. Herrero, A. Aldaz and J. M. Feliu, *Phys. Chem. Chem. Phys.*, 2012, **14**, 10258–10265.
121 Y. Tang, R. E. Edelmann and S. Zou, *Nanoscale*, 2014, **6**, 5630–5633.
122 H. Meng, C. X. Wang, P. K. Shen and G. Wu, *Energy Environ. Sci.*, 2011, **4**, 1522–1526.
123 M. Shao, J. Odell, M. Humbert, T. Yu and Y. Xia, *J. Phys. Chem. C*, 2013, **117**, 4172–4180.
124 B. J. Kim, K. Kwon, C. K. Rhee, J. Han and T. H. Lim, *Electrochim. Acta*, 2008, **53**, 7744–7750.
125 A. Saez, E. Exposito, J. Solla-Gullon, V. Montiel and A. Aldaz, *Electrochim. Acta*, 2012, **63**, 105–111.

126 A. Lopez-Cudero, F. J. Vidal-Iglesias, J. Solla-Gullon, E. Herrero, A. Aldaz and J. M. Feliu, *Phys. Chem. Chem. Phys.*, 2009, **11**, 416–424.
127 S. Uhm, H. J. Lee, Y. Kwon and J. Lee, *Angew. Chem., Int. Ed.*, 2008, **47**, 10163–10166.
128 Q.-S. Chen, Z.-Y. Zhou, F. J. Vidal-Iglesias, J. Solla-Gullón, J. M. Feliu and S.-G. Sun, *J. Am. Chem. Soc.*, 2011, **133**, 12930–12933.
129 H.-X. Liu, N. Tian, M. P. Brandon, J. Pei, Z.-C. Huangfu, C. Zhan, Z.-Y. Zhou, C. Hardacre, W.-F. Lin and S.-G. Sun, *Phys. Chem. Chem. Phys.*, 2012, **14**, 16415–16423.
130 C. Buso-Rogero, J. V. Perales-Rondon, M. J. S. Farias, F. J. Vidal-Iglesias, J. Solla-Gullon, E. Herrero and J. M. Feliu, *Phys. Chem. Chem. Phys.*, 2014, **16**, 13616–13624.
131 J. K. Lee, H. Jeon, S. Uhm and J. Lee, *Electrochim. Acta*, 2008, **53**, 6089–6092.
132 X. W. Yu and P. G. Pickup, *Electrochim. Acta*, 2010, **55**, 7354–7361.
133 X. W. Yu and P. G. Pickup, *J. Appl. Electrochem.*, 2011, **41**, 589–597.
134 B. Peng, J. Y. Wang, H. X. Zhang, Y. H. Lin and W. B. Cai, *Electrochem. Commun.*, 2009, **11**, 831–833.
135 S.-H. Wang, H.-X. Zhang and W.-B. Cai, *J. Power Sources*, 2012, **212**, 100–104.
136 N. Kristian, Y. S. Yan and X. Wang, *Chem. Commun.*, 2008, 353–355.
137 N. Kristian, Y. L. Yu, P. Gunawan, R. Xu, W. Q. Deng, X. W. Liu and X. Wang, *Electrochim. Acta*, 2009, **54**, 4916–4924.
138 J. S. Huang, H. Q. Hou and T. Y. You, *Electrochem. Commun.*, 2009, **11**, 1281–1284.
139 Y. C. Bai, W. D. Zhang, C. H. Chen and J. Q. Zhang, *J. Alloys Compd.*, 2011, **509**, 1029–1034.
140 Y. Y. Huang, S. Y. Zheng, X. J. Lin, L. Q. Su and Y. L. Guo, *Electrochim. Acta*, 2012, **63**, 346–353.
141 Y. J. Kang, L. Qi, M. Li, R. E. Diaz, D. Su, R. R. Adzic, E. Stach, J. Li and C. B. Murray, *ACS Nano*, 2012, **6**, 2818–2825.
142 L. R. Alden, D. K. Han, F. Matsumoto, H. D. Abruna and F. J. DiSalvo, *Chem. Mater.*, 2006, **18**, 5591–5596.
143 F. Matsumoto, C. Roychowdhury, F. J. DiSalvo and H. D. Abruna, *J. Electrochem. Soc.*, 2008, **155**, B148–B154.
144 X. W. Yu and P. G. Pickup, *Electrochim. Acta*, 2011, **56**, 4037–4043.
145 V. Radmilovic, H. Gasteiger and P. Ross, *J. Catal.*, 1995, **154**, 98–106.
146 K. Wang, H. Gasteiger, N. Markovic and P. Ross Jr, *Electrochim. Acta*, 1996, **41**, 2587–2593.
147 Y. Chen, Y. M. Zhou, Y. W. Tang and T. H. Lu, *J. Power Sources*, 2010, **195**, 4129–4134.
148 T. T. Cheng and E. L. Gyenge, *J. Electrochem. Soc.*, 2008, **155**, B819–B828.
149 J. H. Jiang and A. Kucernak, *J. Electroanal. Chem.*, 2009, **630**, 10–18.
150 J. H. Choi, K. J. Jeong, Y. Dong, J. Han, T. H. Lim, J. S. Lee and Y. E. Sung, *J. Power Sources*, 2006, **163**, 71–75.
151 Z. L. Liu and L. Hong, *J. Appl. Electrochem.*, 2007, **37**, 505–510.
152 C. Li and Y. Yamauchi, *Phys. Chem. Chem. Phys.*, 2013, **15**, 3490–3496.
153 Y. Jia, Y. Jiang, J. Zhang, L. Zhang, Q. Chen, Z. Xie and L. Zheng, *J. Am. Chem. Soc.*, 2014, **136**, 3748–3751.
154 V. Mazumder and S. H. Sun, *J. Am. Chem. Soc.*, 2009, **131**, 4588–4589.
155 V. Mazumder, M. F. Chi, M. N. Mankin, Y. Liu, O. Metin, D. H. Sun, K. L. More and S. H. Sun, *Nano Lett.*, 2012, **12**, 1102–1106.
156 M. Chen, Z. B. Wang, K. Zhou and Y. Y. Chu, *Fuel Cells*, 2010, **10**, 1171–1175.
157 L. L. Zhang, T. H. Lu, J. C. Bao, Y. W. Tang and C. Li, *Electrochem. Commun.*, 2006, **8**, 1625–1627.
158 Y. Zhu, Y. Y. Kang, Z. Q. Zou, Q. Zhou, J. W. Zheng, B. J. Xia and H. Yang, *Electrochem. Commun.*, 2008, **10**, 802–805.
159 X. M. Wang and Y. Y. Xia, *Electrochim. Acta*, 2009, **54**, 7525–7530.
160 H. Q. Li, G. Q. Sun, Q. A. Jiang, M. Y. Zhu, S. Sun and Q. Xin, *Electrochem. Commun.*, 2007, **9**, 1410–1415.
161 N. C. Cheng, H. F. Lv, W. Wang, S. C. Mu, M. Pan and F. Marken, *J. Power Sources*, 2010, **195**, 7246–7249.
162 J. Ge, W. Xing, X. Xue, C. Liu, T. Lu and J. Liao, *J. Phys. Chem. C*, 2007, **111**, 17305–17310.
163 Z. Y. Bai, L. Yang, L. Li, J. Lv, K. Wang and J. Zhang, *J. Phys. Chem. C*, 2009, **113**, 10568–10573.
164 R. Li, H. Hao, W.-B. Cai, T. Huang and A. Yu, *Electrochem. Commun.*, 2010, **12**, 901–904.
165 Y. Y. Jiang, Y. Z. Lu, D. X. Han, Q. X. Zhang and L. Niu, *Nanotechnology*, 2012, **23**, 105609.
166 D. Li, C. Wang, D. Tripkovic, S. Sun, N. M. Markovic and V. R. Stamenkovic, *ACS Catal.*, 2012, 1358–1362.
167 X. L. Ji, K. T. Lee, R. Holden, L. Zhang, J. J. Zhang, G. A. Botton, M. Couillard and L. F. Nazar, *Nat. Chem.*, 2010, **2**, 286–293.
168 Z. Y. Bai, Y. M. Guo, L. Yang, L. Li, W. J. Li, P. L. Xu, C. G. Hu and K. Wang, *J. Power Sources*, 2011, **196**, 6232–6237.
169 S. D. Yang, X. G. Zhang, H. Y. Mi and X. G. Ye, *J. Power Sources*, 2008, **175**, 26–32.
170 M. Zheng, P. Li, G. Fu, Y. Chen, Y. Zhou, Y. Tang and T. Lu, *Appl. Catal., B*, 2013, **129**, 394–402.
171 C. G. Hu, Z. Y. Bai, L. Yang, J. Lv, K. Wang, Y. M. Guo, Y. X. Cao and J. G. Zhou, *Electrochim. Acta*, 2010, **55**, 6036–6041.
172 O. Winjobi, Z. Y. Zhang, C. H. Liang and W. Z. Li, *Electrochim. Acta*, 2010, **55**, 4217–4221.
173 C. H. Chen, W. J. Liou, H. M. Lin, S. H. Wu, A. Borodzinski, L. Stobinski and P. Kedzierzawski, *Fuel Cells*, 2010, **10**, 227–233.
174 S. Zhang, Y. Y. Shao, H. G. Liao, M. H. Engelhard, G. P. Yin and Y. H. Lin, *ACS Nano*, 2011, **5**, 1785–1791.
175 S. Zhang, Y. Y. Shao, H. G. Liao, J. Liu, I. A. Aksay, G. P. Yin and Y. H. Lin, *Chem. Mater.*, 2011, **23**, 1079–1081.
176 C. V. Rao, C. R. Cabrera and Y. Ishikawa, *J. Phys. Chem. C*, 2011, **115**, 21963–21970.
177 S. Bong, S. Uhm, Y. R. Kim, J. Lee and H. Kim, *Electrocatalysis*, 2010, **1**, 139–143.

178 S. D. Yang, C. M. Shen, X. J. Lu, H. Tong, J. J. Zhu, X. G. Zhang and H. J. Gao, *Electrochim. Acta*, 2012, **62**, 242–249.
179 C. M. Miesse, W. S. Jung, K. J. Jeong, J. K. Lee, J. Lee, J. Han, S. P. Yoon, S. W. Nam, T. H. Lim and S. A. Hong, *J. Power Sources*, 2006, **162**, 532–540.
180 S. Ha, R. Larssen, Y. Zhu and R. I. Masel, *Fuel Cells*, 2004, **4**, 337–343.
181 S. Ha, Z. Dunbar and R. I. Masel, *J. Power Sources*, 2006, **158**, 129–136.
182 J. Chang, L. Feng, C. Liu, W. Xing and X. Hu, *Angew. Chem., Int. Ed.*, 2014, **53**, 122–126.
183 R. Wang, J. Liu, P. Liu, X. Bi, X. Yan, W. Wang, X. Ge, M. Chen and Y. Ding, *Chem. Sci.*, 2014, **5**, 403–409.
184 R. Wang, J. Liu, P. Liu, X. Bi, X. Yan, W. Wang, Y. Meng, X. Ge, M. Chen and Y. Ding, *Nano Res.*, 2014, DOI: 10.1007/s12274-014-0517-9.
185 W. Cai, L. Yan, C. Li, L. Liang, W. Xing and C. Liu, *Int. J. Hydrogen Energy*, 2012, **37**, 3425–3432.
186 P. Hong, S. J. Liao, J. H. Zeng and X. J. Huang, *J. Power Sources*, 2010, **195**, 7332–7337.
187 P. Hong, S. J. Liao, J. H. Zeng, Y. L. Zhong and Z. X. Liang, *J. Power Sources*, 2011, **196**, 1107–1111.
188 P. Hong, Y. Zhong, S. Liao, J. Zeng, X. Lu and W. Chen, *J. Power Sources*, 2011, **196**, 5913–5917.
189 E. Kjeang, N. Djilali and D. Sinton, *J. Power Sources*, 2009, **186**, 353–369.
190 S. A. Mousavi Shaegh, N.-T. Nguyen and S. H. Chan, *Int. J. Hydrogen Energy*, 2011, **36**, 5675–5694.
191 J. Ma, A. S. Gagoa and N. Alonso-Vante, *J. Electrochem. Soc.*, 2013, **160**, F859–F866.
192 X. Zhu, B. Zhang, D.-D. Ye, J. Li and Q. Liao, *J. Power Sources*, 2014, **247**, 346–353.
193 H. S. Kim, R. D. Morgan, B. Gurau and R. I. Masel, *J. Power Sources*, 2009, **188**, 118–121.
194 H. Qiao, H. Shiroishi and T. Okada, *Electrochim. Acta*, 2007, **53**, 59–65.
195 R. Chenitz and J. P. Dodelet, *J. Electrochem. Soc.*, 2010, **157**, B1658–B1664.
196 P. Hong, F. Luo, S. J. Liao and J. H. Zeng, *Int. J. Hydrogen Energy*, 2011, **36**, 8518–8524.
197 W. W. Cai, L. Yan, C. Y. Li, L. Liang, W. Xing and C. P. Liu, *Int. J. Hydrogen Energy*, 2012, **37**, 3425–3432.
198 A. Saez, J. Solla-Gullon, E. Exposito, A. Aldaz and V. Montiel, *Int. J. Electrochem. Sci.*, 2013, **8**, 7030–7043.
199 Y. Y. Kang, M. J. Ren, T. Yuan, Y. J. Qiao, Z. Q. Zoa and H. Yang, *J. Power Sources*, 2010, **195**, 2649–2652.
200 Y. Y. Kang, M. J. Ren, Z. Q. Zou, Q. H. Huang, Z. L. Li, D. L. Akins and H. Yang, *Electrochim. Acta*, 2010, **55**, 5274–5280.
201 R. D. Morgan, J. L. Haan and R. I. Masel, *J. Power Sources*, 2010, **195**, 6405–6410.
202 S. M. Baik, J. Kim, J. Han and Y. Kwon, *Int. J. Hydrogen Energy*, 2011, **36**, 12583–12590.
203 S. Uhm, Y. Kwon, S. T. Chung and J. Lee, *Electrochim. Acta*, 2008, **53**, 5162–5168.
204 W. W. Cai, L. Liang, Y. W. Zhang, W. Xing and C. P. Liu, *Int. J. Hydrogen Energy*, 2013, **38**, 212–218.